OFFICE OF NAVAL RESEARCH

Research Contract N00014-83-K-0343

Technical Report No. 66

OXYGEN REDUCTION ON ADSORBED IRON TETRAPYRIDINO PORPHYRAZINE

By

A.A. Tanaka, C. Fierro, D.A. Scherson and E. Yeager

Prepared for Publication

in the

Materials Chemistry and Physics

Case Center for Electrochemical Sciences
and the Department of Chemistry
Case Western Reserve University
Cleveland, Ohio 44106-2699

1 September 1988

UNCLASSIFIED
SECURITY CLASSIFICATION OF THIS PAGE

REPORT DOCUMENTATION PAGE

1a. REPORT SECURITY CLASSIFICATION: unclassified	1b. RESTRICTIVE MARKINGS
2a. SECURITY CLASSIFICATION AUTHORITY	3. DISTRIBUTION / AVAILABILITY OF REPORT: Approved for public release and sale; its distribution is unlimited
2b. DECLASSIFICATION / DOWNGRADING SCHEDULE	
4. PERFORMING ORGANIZATION REPORT NUMBER(S): Technical Report No. 66	5. MONITORING ORGANIZATION REPORT NUMBER(S)
6a. NAME OF PERFORMING ORGANIZATION: Case Western Reserve University; 6b. OFFICE SYMBOL (If applicable)	7a. NAME OF MONITORING ORGANIZATION: ONR Chemistry Program
6c. ADDRESS (City, State, and ZIP Code): Cleveland, Ohio 44106	7b. ADDRESS (City, State, and ZIP Code): Arlington, Virginia 22217-5000
8a. NAME OF FUNDING / SPONSORING ORGANIZATION: Office of Naval Research; 8b. OFFICE SYMBOL (If applicable)	9. PROCUREMENT INSTRUMENT IDENTIFICATION NUMBER: Contract N00014-83-K-0343
8c. ADDRESS (City, State, and ZIP Code): Arlington, Virginia 22217	10. SOURCE OF FUNDING NUMBERS: PROGRAM ELEMENT NO. / PROJECT NO. NR359 451 / TASK NO. / WORK UNIT ACCESSION NO

11. TITLE (Include Security Classification): Oxygen Reduction on Adsorbed Iron Tetrapyridino Porphyrazine

12. PERSONAL AUTHOR(S): A.A. Tanaka, C. Fierro, D.A. Scherson and E. Yeager

13a. TYPE OF REPORT	13b. TIME COVERED	14. DATE OF REPORT (Year, Month, Day)	15. PAGE COUNT
Technical Report	FROM 1987 TO 1988	September 1, 1988	43

16. SUPPLEMENTARY NOTATION

17 COSATI CODES		
FIELD	GROUP	SUB-GROUP

18. SUBJECT TERMS (Continue on reverse if necessary and identify by block number): oxygen reduction, electrocatalysts, transition metal macrocycles, tetrapyridino porphyrazine

19. ABSTRACT (Continue on reverse if necessary and identify by block number)

The electrocatalytic properties of iron tetrapyridino porphyrazine FeTPyPz for the reduction of $O_2^?$ in alkaline media have been examined with cyclic voltammetry and rotating ring disk techniques. Four distinct redox peaks are observed in the absence of $O_2^?$ in solution for this material adsorbed at monolayer coverages on ordinary pyrolytic graphite surfaces. The onset for $O_2^?$ reduction appears to coincide with the voltammetric peak associated with the metal centered Fe(II)TPyPz/Fe(III)TPyPz transition. No hydrogen peroxide is detected at the ring in this potential range indicating that the reaction takes place by a four electron pathway. This is in contrast with the behavior observed at more negative potentials for which sizable currents for $H_2O_2^?$ oxidation are observed. This change in the mechanism has been attributed to the further reduction of the iron center in the macrocycle rendering an Fe(I)TPyPz species. If the electrode is polarized at potentials more negative than -0.8 V vs SCE, however, the reduction proceeds once again without generation of $H_2O_2^?$ in the solution phase. Quantum mechanical arguments involving orbital symmetry and (CONTINUED ON NEXT PAGE)

20 DISTRIBUTION / AVAILABILITY OF ABSTRACT	21 ABSTRACT SECURITY CLASSIFICATION
☒ UNCLASSIFIED/UNLIMITED ☐ SAME AS RPT ☐ DTIC USERS	unclassified
22a NAME OF RESPONSIBLE INDIVIDUAL: Ernest Yeager, Professor of Chemistry	22b TELEPHONE (Include Area Code): (216) 368-3626; 22c. OFFICE SYMBOL

DD FORM 1473, 84 MAR — 83 APR edition may be used until exhausted. All other editions are obsolete.

SECURITY CLASSIFICATION OF THIS PAGE
UNCLASSIFIED

September 1, 1988

Office of Naval Research
Chemistry Program
Contract N00014-83-K-0343
Project No. NR459 451

Abstract (Continued)

overlap indicate that the activation could involve a simultaneous bonding of O_2 to the iron center and a bridge nitrogen in the macrocycle ring. Such a potential dependent mechanism is similar to that reported earlier for iron tetrasulfonated phthalocyanine for which theoretically predicted electronic properties are essentially the same as those of FeTPyPz.

OXYGEN REDUCTION ON ADSORBED IRON TETRAPYRIDINOPORPHYRAZINE

by

A.A. Tanaka,† C. Fierro, D. A. Scherson and E. Yeager
Case Center for Electrochemical Sciences
and the Chemistry Department
Case Western Reserve University
Cleveland, Ohio 44106

ABSTRACT

The electrocatalytic properties of iron tetrapyridino porphyrazine FeTPyPz for the reduction on O_2 in alkaline media have been examined with cyclic voltammetry and rotating ring disk techniques. Four distinct redox peaks are observed in the absence of O_2 in solution for this material adsorbed at monolayer coverages on ordinary pyrolytic graphite surfaces. The onset for O_2 reduction appears to coincide with the voltammetric peak associated with the metal centered Fe(II)TPyPz/Fe(III)TPyPz transition. No hydrogen peroxide is detected at the ring in this potential range indicating that the reaction takes place by a four electron pathway. This is in contrast with the behavior observed at more negative potentials for which sizable currents for H_2O_2 oxidation are observed. This change in the mechanism has been attributed to the further reduction of the iron center in the macrocycle rendering an Fe(I)TPyPz species. If the electrode is polarized at potentials more negative than -0.8 V vs SCE, however, the reduction proceeds once again without generation of H_2O_2 in the solution phase. Quantum mechanical arguments involving orbital symmetry and overlap indicate that the activation could involve a simultaneous bonding of O_2 to the iron center and a bridge nitrogen in the macrocycle ring. Such a potential dependent mechanism is similar to that reported earlier for iron tetrasulfonated phthalocyanine for which theoretically predicted electronic properties are essentially the same as those of FeTPyPz.

---

†Permanent address: Instituto de Fisica e Quimica de Sao Carlos-USP, Sao Carlos, (SP), Brazil.

INTRODUCTION

Iron and cobalt macrocycles have been extensively studied over the past two decades as catalysts for the electrochemical reduction of dioxygen.[1-10] The importance of such investigations is two-fold. First, the high activity exhibited by some of these compounds has opened the possibility of replacing platinum in fuel cell applications and second, a systematic examination of the electrocatalytic reduction of O_2 by transition metal macrocycles in general may provide further insight into the factors involved in the overall phenomenon of O_2 activation.

This paper focuses attention on the modification in the mechanism of O_2 reduction induced by changes in the oxidation state of a specific macrocycle. An iron pyridinoporphyrazine FeTPyPz (see Fig. 1) was selected for this study on the basis of the following considerations: i) this compound undergoes irreversible adsorption on ordinary pyrolytic graphite surfaces from acid solutions and its electrochemical characteristics as an adsorbed layer can be studied without it being present in the solution phase; ii) quantum mechanical calculations performed in this laboratory[11] provide evidence that the ability of FeTPyPz to reduce O_2 should be similar to that of iron tetrasulfonated phthalocyanine (FeTsPc) whose electrochemical properties have been thoroughly investigated[7,12], thus providing a means of making a reliable comparison between theory and experiment; and iii) both FeTsPc and FeTPyPz exhibit multiple voltammetric peaks in the region of O_2 reduction.

EXPERIMENTAL

Synthesis

The iron tetra-2,3-pyridinoporphyrazine was synthesized and purified according to the method reported by Smith et al.[13] A finely ground homogeneous mixture of 2,3-pyridinedicarboxylic acid (2.0 g; 1.1×10^{-2} mole, Aldrich), urea

(6.4 g; 0.11 mole, Fisher), and ammonium molybdate (0.25g; 2.02×10^{-4} mole, Matheson Colleman & Bell) was slowly added to 1,2,4-trichlorobenzene (80 ml, Fischer) at 150-160°C under a nitrogen atmosphere. After 1 h, iron(II) oxalate (2.2 g; 1.22×10^{-2} mole, Johnson Matthey) was added to the mixture. The temperature was then raised to 200-210°C and maintained in this range for 4 h. The crude product was ground with a mortar and pestle and washed successively with benzene, ethanol, hot water, warm 5% w/v NaOH, hot water, warm 2.5 % v/v HCl, and, finally, hot water. The remaining product was further purified by dissolving it in concentrated sulfuric acid, filtering in a sintered glass funnel, and precipitating with an ice bath. The final product was collected by centrifugation, washed thoroughly with hot water, and finally dried overnight at 65°C under vacuum. For FeTPyPz ($C_{28}H_{12}N_8Fe$).$2H_2O$, the elemental analysis* in weight percents was as follows:

	Weight percent			
	C	H	N	Fe
Calculated:	55.00	2.65	27.50	9.18
Experimental:	52.50	2.90	26.63	10.93

Since the water of hydration is not expected to be stiochiometric, the N/C and Fe/C ratios are more significant; i.e.,

	N/C	Fe/C
Calculated:	0.500	0.167
Experimental:	0.507	0.208

The experimental value for N/C is reasonable but that for Fe/C is too high by ~25%. This may be due to the presence of some iron as a salt, perhaps the

The iron tetrasulfonated phthalocyanine was prepared according to the procedure of Weber and Busch[14]. Monosodiun salt of 4-sulfophthalic acid was sul

*The elemental analyses were performed by Galbraith Laboratories, Knoxville, TN.

obtained by reaction of NaOH with aqueous 50% 4-sulfophthalic acid (Eastman Kodak) and then twice recrystallized by using water-acetone mixtures. Ferrous acetate 7-hydrate (13.5 g, 0.048 mole, Aldrich), urea (58.0 g, 0.97 mole, Fisher), ammonium chloride (4.7 g, 0.09 mole, J.T. Baker), monosodium salt of sulfophthalic acid (43.2 g, 0.162 mole), and ammonium molybdate 4-hydrate (0.69 g, 5.6×10^{-4} M, Matheson Colleman & Bell) were ground together. The mixture was added slowly to nitrobenzene (40 ml, Mallinckrodt) at 180°C under a nitrogen atmosphere. The reaction was allowed to proceed for 6 hours with the temperature maintained at 170-185°C. The resulting crude product was thoroughly washed with methanol and left overnight in a Soxhlet apparatus for continuous washing with methanol. The remaining solid was put in warm 1 M HCl saturated with NaCl and cooled to room temperature, and the product was obtained by filtration. The product was purified three times by dissolving it in warm 0.1 M NaOH, filtering, and reprecipitating it with addition of excess NaCl. The compound was washed with 80% v/v aqueous ethanol until the filtrate was chloride free (checked with $AgNO_3$ solution) and washed overnight with refluxing absolute ethanol. The final product was dried at 60°C under vacuum for 2 days. For $C_{32}H_{12}N_8O_{12}S_4Na_4Fe.H_2O$:

Weight percent

	C	H	N	S	Fe
Calculated:	38.65	1.42	11.27	12.89	5.62
Experimental:	38.74	3.32	11.16	12.77	7.70

The calculated and experimentally found weight ratios were as follows:

Weight percent

	N/C	S/C	Fe/C	Fe/N	Fe/S
Calculated:	0.292	0.334	0.145	0.499	0.436
Experimental+:	0.288	0.330	0.199	0.690	0.603

The N/C and S/C weight ratios found experimentally are close to the theoretical value but the experimental Fe/C, Fe/N and Fe/S ratios are all high by

~30%. As with the FeTPyPz, this probably indicates that some of the iron is in the form of salts and/or oxides despite the purification procedures. Anions may be also included in the TsPc crystal structure.

Electrochemical Measurements

Cyclic voltammetry experiments were conducted with an ordinary pyrolytic graphite, OPG (Union Carbide Co., Parma, OH), in the form of a disk (OD= 0.5 cm) molded in Kel-F. The potential was monitored with a Princeton Applied Research (PARC) Model 175/176 system.

Rotating gold ring (O.D.= 0.714 cm, I.D.= 0.554 cm)- OPG disk (D = 0.5 cm) oxygen reduction polarization curves were recorded in the dynamic polarization mode at a sweep rate of 10 mV/s with a Pine Model RDE-3 double potentiostat. A value of 0.38 was calculated for the collection efficiency (N) of the ring from the geometry of the electrode and using the table of Albery and Bruckenstein[15]. The gold ring was activated before recording each polarization curve by cycling between potentials high enough to oxidize organic and underpotential deposited impurities (+0.4 V vs. SCE) and sufficiently negative to reduce the oxide layer formed (-1.0 V vs. SCE). It was then polarized at +0.1 V vs. SCE, a potential well within the diffusion controlled region for the oxidation of hydrogen peroxide in 0.1 M NaOH.[16]

A three-compartment conventional electrochemical cell was used. A gold foil (A ~ 2 cm^2) and a saturated calomel electrode (SCE) served as the counter and reference electrode, respectively. The final polishing for the disk electrode was performed with 0.05 μm alumina suspended in water. It was then washed washed with water and 0.05 M H_2SO_4 under ultrasonic agitation with a final rinse with water. It was then immediately introduced into the electrochemical cell or dipped in a solution containing the catalyst for adsorption. The catalyst was adsorbed onto the graphite surface by immersing the electrodes

in an air-saturated solution 10^{-4} M FeTPyPz in 0.1 M H_2SO_4 and then rotating it at ~100 rpm for ~20 min. The electrode was then thoroughly rinsed with purified water and introduced into the electrochemical cell.

All solutions were prepared with water purified with a reverse osmosis and distillation system[17]. The following solutions were used: 0.05 M H_2SO_4 (ULTREX, J.T. Baker); 0.1 M NaOH (special low in carbonate, J.T. Baker); NaOH/$NaHPO_4$ (Fisher), (pH 11.5); Na_2CO_3 (Fisher)/$NaHCO_3$ (Fisher), (pH 10.5); H_3BO_3 (Fisher)/$Na_2B_4O_7.10H_2O$ (Fisher), (pH 8.4), NaOH/KH_2PO_4 (Fisher), (pH 7.0), NaOH/$KHC_8H_4O_4$ (Fisher), (pH 5.0); NaOH/$C_6H_8O_7$ (Fisher), (pH 2.9). The pH of the solutions was measured with a Orion Model 701A pH meter.

RESULTS AND DISCUSSION

Cyclic Voltammetry Measurements

Ordinary pyrolytic graphite (OPG) was used as an inert substrate to examine the electrochemical properties of the macrocycles. Figure 2 shows the voltammetry obtained in a deareated 0.1 M NaOH solution. This featureless voltammogram indicates that the currents observed are essentially of a non-faradaic nature (i.e., not involving electron transfer). At potentials more positive than ~+0.6 V vs. SCE an increase in the current can be observed and probably corresponds to the onset for oxygen evolution. In the cathodic limit (~-1.4 V vs. SCE), a rounded shape can be noted in the voltammogram following the reversal of the sweep suggesting a faradaic contribution; possibly involving surface functional groups which respond slowly to the change in potential. The tilt of the voltammetry curve in Fig. 2 is probably due to either solution filled microfissures in the OPG surface or slight penetration of electrolytic solution between the side of the OPG disk and the Kel-F, most likely the former explanation.

The non-faradaic current (i_{nf}) is related to the differential double-layer

capacity (C_d) by the equation:[18]

$$i_{nf} = C_d \left(\frac{dE}{dt}\right) \quad (1)$$

where (dE/dt) is the potential sweep rate. From eq. 1,

$$\Delta i_{nf} = (i_{nf})_a - (i_{nf})_c = 2\, C_d\, v \quad (2)$$

where v is the sweep rate and the subscripts a and c correspond to anodic and cathodic, respectively. Using eq. 2 and the voltammetry curve in Fig. 2 the average value for the apparent differential capacity is of the order of 50 μF cm^{-2}. The value of the capacity at the minimum of the capacity-potential curves for similar electrode material has been determined by Randin and Yeager[19] in 0.9 M NaF at 25°C and 1000 Hz, and a minimum value of 18 μF cm^{-2} has been found in the capacitance vs. potential curve. Bauer et al.[20] have observed a minimum value of ~60 μF cm^{-2} for OPG in 0.5 M KCl at 1000 Hz. The higher value observed in the present work and that of Bauer et al. compared with 18 μF cm^{-2} is probably caused by differences in the preparation of the electrode surface, i.e., the electrode area is very sensitive to the polishing procedure since flakes of graphite polished into the surface can produce a significant variation in the actual area. In addition, as pointed out by Randin and Yeager,[19] surface imperfections and impurities in the electrolyte may also affect the capacity value.

Typical cyclic voltammograms of FeTPyPz pre-adsorbed on OPG surface in deareated 0.1 M NaOH solution are shown in Fig. 3. Three redox processes (labelled 1, 2, and 3) are observed and the respective charges, estimated from the area under the peaks involved are ~50, 16 and 17 $\mu C/cm^2$. These charges are in good agreement with those reported by Zecevic et al.[12] and Zagal et al.[7] for FeTsPc on OPG. The peak currents are directly proportional to the sweep rate over the range investigated (50-500 mV/s) and the peak potential separations ($E_{p,anodic} - E_{p,cathodic}$) are very small (~10 mV for the highest scan rate) for

all peaks. These observations indicate that the redox processes are due to faradaic processes involving adsorbed species.[18]

Of particular interest is the number of electrons (n) involved in each of the redox peaks shown in Fig. 3. For a given peak, assuming ideal Nernstian behavior, the peak current (i_p) can be related to the potential scan rate (v) by the equation:[18]

$$i_p = \left(\frac{n^2F^2}{4RT} \right) \cdot v \cdot A \cdot \Gamma \qquad (3)$$

where Γ is the total surface concentration of the adsorbed species (mol. cm^{-2}), A is the electrode area (cm^2), and the other terms have their usual meanings. The total surface concentration of the adsorbed species (Γ) is related to the charge (Q) under the voltammetric peak by:[18]

$$Q = n \cdot F \cdot A \cdot \Gamma \qquad (4)$$

Thus, the number of electrons (n) involved in each redox process can be evaluated using the equation:

$$n = \frac{4RT}{vF} \cdot \frac{i_p}{Q} \qquad (5)$$

Experimental values of i_p and Q yield values of 1.4, 0.95, and 1.0 for the peaks 1, 2, and 3, respectively, indicating that one electron per molecule is involved in each of the surface redox processes. The deviation from a value of 1 can probably be attributed to the non-ideality of the system.[18] From Eq. 4 and with the assumption of 1 electron/molecule, the charges under peaks 2 and 3 lead to about 1.74×10^{-10} mole cm^{-2} of adsorbed metal complex. If we assume that the macrocycle has an area of ~200 $Å^2$ and each molecule lies flat on the electrode surface[16], the coverage by adsorbed species corresponds to approximately a monolayer. If the complex is adsorbed edge-on[1] as proposed for FeTsPc on silver by Simic-Glavaski et al.,[12] then this charge corresponds to ~0.5 of a

monolayer.

The electrochemical properties of FeTsPc pre-adsorbed on graphite surfaces were studied by Zagal et al.[7] in aqueous solutions and two voltammetric peaks associated with the metal center were reported. Later, Zecevic et al.[12] observed two more peaks involving reduction and oxidation of the macrocycle ring on OPG electrodes in dilute aqueous solutions of FeTsPc (10^{-5} M) in which only features corresponding to the adsorbed species are obtained. The similarity between the voltammetric behavior of FeTPyPz and FeTsPc, as shown in Fig. 4, led to the investigation of the dependence of the multiple redox processes on pH for both compounds shown in Fig. 5. In most instances, an approximate -60 mV/pH unit dependence was observed indicating that one proton or one hydroxyl group is involved in a particular redox couple equilibrium.

On the basis of electrochemical studies involving FeTsPc[7,12] and the water soluble iron tetra(4-N-methylpyridyl)porphyrin FeTMPyP,[21,22] peak 3 in Fig. 4 can be assigned to the redox process Fe(III)/Fe(II). At pH > 4, a 60 mV/pH unit dependence is observed (see Fig. 5) and most probably corresponds to the reaction:

$$\begin{array}{l} H_2O \\ | \\ Fe(III)TPyPz(-2) \\ | \\ OH \end{array} + e^- + H_2O = \begin{array}{l} H_2O \\ | \\ Fe(II)TPyPz(-2) \\ | \\ H_2O \end{array} + OH^- \qquad (6)$$

In more acid media (pH < 4), the redox process become pH independent and given by

$$\begin{array}{l} H_2O \\ | \\ [Fe(III)TPyPz(-2)]^+ \\ | \\ H_2O \end{array} + e^- = \begin{array}{l} H_2O \\ | \\ Fe(II)TPyPz(-2) \\ | \\ H_2O \end{array} \qquad (7)$$

Reactions 6 and 7 suggest that a proton equilibrium exists between the ferric species, i.e.,

$$\begin{array}{l} H_2O \\ | \\ [Fe(III)TPyPz(-2)]^+ \end{array} + H_2O = \begin{array}{l} H_2O \\ | \\ Fe(III)TPyPz(-2) \\ | \\ OH \end{array} + H^+ \qquad (8)$$

with a pK_a value of ca. 4, in agreement with the results of Zagal et al.[7] A pK_a of 4.7 has also been observed for the positively charged Fe(III)TMPyP.[21,22]

Peak 2 in Fig. 4 appears to be associated with the redox process Fe(II)/Fe(I), as previously suggested for FeTsPc.[7,12] The formation of Fe(I) species has also been suggested for iron phthalocyanine[23-25] on the basis of electrochemical measurements. At pH < 7, the dependence of the peak 2 on the pH is ~60 mV/pH unit (see Fig. 5) and most likely can be described as

$$\begin{array}{l} H_2O \\ | \\ Fe(II)TPyPz(-2) \\ | \\ H_2O \end{array} + e^- + H^+ = \begin{array}{l} H_2O \\ | \\ [Fe(I)TPyPz(-2)]^-H^+ \\ | \\ H_2O \end{array} \qquad (9)$$

with the proton in this case, most likely, sitting on a bridging azo nitrogen atom. At pH above 7, the redox process becomes pH independent, i.e.,

$$\begin{array}{l} H_2O \\ | \\ Fe(II)TPyPz(-2) \\ | \\ H_2O \end{array} + e^- = \begin{array}{l} H_2O \\ | \\ [Fe(I)TPyPz(-2)]^- \\ | \\ H_2O \end{array} \qquad (10)$$

The macrocycle ring in its normal oxidation state carries two negative charges, P(-2) where P represents the ring. Zecevic et al.[12] have proposed that the peaks 1 and 4 for FeTsPc in Fig. 4 are most likely associated with the ring reduced form [anion radical, P(-3)] and the oxidized form [cation radical, P(-1)], respectively. Peak 4, however, may involve an Fe(IV) species rather than an Fe(III) radical cation. The pH dependence of peak 1 (see Fig.

5) shows a discontinuity near pH 6. In the case of FeTsPc, this has been attributed[12] to a rapid changeover from deprotonated (basic media) to all protonated (acid media) sulfonic groups; however, such an explanation is not applicable for FeTPyPz. The voltammetry curves in both cases suggest that the process is reversible and, perhaps, at this pH value and this very negative potential dimerization and/or anion effects play an important role. The present data, however, does not provide evidence for dimeric species participation and there is controversy in the literature if bridging groups such as μ-oxo, μ-hydroxy, or μ-dihydroxyl are involved. Breakdown of the dimer has been reported to occur in the pH range 6-7 for FeTMPyP[21,22] and also for iron tetrasulfonated phenyl porphyrin[26] (FeTsPP).

As mentioned before, the charge under peak 1 in Figs. 3 and 4 is much larger than that under the other peaks, even though all of the redox processes appear to involve one electron. The same feature has been observed for FeTsPc[12] and it has been proposed that perhaps the macrocycle is present in stacks on the surface and that at potential corresponding to peak 1 the number of electroactive species is much greater than for the other redox processes at more positive potentials. In the solution phase both metal-free TMPyP and metal-free TPyP exhibit a quasi-reversible process at ~+0.13 V vs. NHE and a second irreversible reduction wave at -0.4 V vs. NHE involving two- and four-electron, respectively, based on i_p vs. $v^{1/2}$ analysis.[22] Furthermore, six electrons also appear to be involved to fully reduce metal-free TMPyP at -0.4 V vs. NHE based on thin-layer coulometric experiments.[23] For the adsorbed species, a multi-electron transfer process is possible at a given potential but seems very unlikely in view of the n value of one obtained from Eq. 5.

Another possibility is that the solution phase contains some of the de-metallized macrocycle which could also adsorbed on the electrode surface at a higher surface coverage than the metallized complex.

Oxygen Reduction Measurements

Oxygen Reduction on Ordinary Pyrolytic Graphite Substrate

Figure 6 shows the rotating ring-disk polarization curves for oxygen reduction on OPG in 0.1 M NaOH solution. The polarization curves are characterized by three regions: the reduction starts at ~-0.25 V vs. SCE and reaches a maximum at ~-0.5 V vs. SCE (region 1), falls to a minimum (region 2, $-0.52 < E < -0.68$ V), and finally increases gradually at more negative potentials (region 3, $E < -0.68$ V).

For the oxygen reduction reaction on the rotating disk electrode, if first-order kinetics with respect to the O_2 diffusing reactant is involved, the observed currents i are related to the rotation rate ω (rad s^{-1}), by the equation:[27-29]

$$\frac{1}{i} = \frac{1}{i_k} + \frac{1}{B \cdot \omega^{1/2}} \qquad (11)$$

where i_k is the kinetic current and B is a constant given as[30]

$$B = n \cdot F \cdot \nu^{1/2} \cdot C_b \left[0.621 \cdot S^{-2/3} / (1 + 0.298 \cdot S^{-1/3} + 0.145 \cdot S^{-2/3}) \right] \qquad (12)$$

where n is the number of electrons per oxygen molecule involved in the faradaic process, F the Faraday constant, ν the kinematic viscosity of the electrolyte (cm^2 s^{-1}), c_b the bulk concentration of oxygen mole cm^{-3}, and S the Schmidt number given by $s = \nu/D$ where D is the diffusion coefficient of O_2 in the media cm^2 s^{-1}).

Equations 11 and 12 involve the assumptions of uniform current distribution and negligible back-reaction contribution. According to Eq. 11, a plot of i^{-1} vs. $f^{-1/2}$, where f is the rotation rate in reciprocal minutes, for various potentials should yield straight lines with the intercepts corresponding to i_k and the slopes to B values.

Figure 7 shows the plot of i^{-1} vs. $f^{-1/2}$ for the reduction of oxygen on the OPG disk electrode in 0.1 M NaOH at different potentials. The linearity and parallelism in this plot provide evidence that the kinetics are first order in O_2 and that Eq. 11 is applicable. This type of plot, however, is not very sensitive to the reaction order. The value of B obtained from this plot is $(1.46 \pm 0.90)\times10^{-2}$ mA $(rpm)^{-1/2}$, which compares favorably with the calculated value of 1.42×10^{-2} mA $(rpm)^{-1/2}$ using Eq. 12 with $n = 2$ and the data of Gubbins and Walker[31] for the diffusion coefficient and solubility of O_2 in 0.1 M NaOH at 22°C.

To analyze the rotating ring-disk electrode data, the general scheme in Fig. 8 for the reduction of oxygen will be considered. In this scheme, oxygen diffusing from the solution to the electrode surface can be electrochemically reduced either to H_2O (k_1) or to H_2O_2 (k_2). The adsorbed hydrogen peroxide, in addition to desorbing and diffusing into the solution (k_5), can be further reduced to H_2O (k_3), oxidized back to O_2 (k'_2), or undergo heterogeneous catalytic decomposition into O_2 and H_2O (k_4). It can be demonstrated[32] that the different first order rate constants (k) are related to the ratio of the ring (i_r) to disk (i_d) currents, as well as the rotation rate ω (rad s^{-1}), by

$$\frac{i_d}{i_r} = \frac{1}{N}\left[1 + \frac{2k_1}{k_2} + X + \left(\frac{k'_5\, X}{Y\, f^{1/2}}\right)\right] \qquad (13)$$

where:

$$X = \left[\left(\frac{2k_1}{k_2k_5}\right)\left(k'_2 + k_3 + k_4\right) + \left(\frac{2k_3 + k_4}{k_5}\right)\right] \qquad (14)$$

and

$$Y = 0.62\, D^{2/3}\, \nu^{-1/6} \qquad (15)$$

A plot of $(i_d/i_r)N$ vs. $f^{-1/2}$ at various fixed potentials is shown in Fig. 9. The value of essentially unity for $(i_d/i_r)N$ over a wide range of potentials and rotation rates indicates that the O_2 is quantitatively reduced to hydrogen peroxide by a two electron pathway on the OPG disk electrode with negligible further reduction or catalytic decomposition of peroxide over the potential range examined.

As pointed out earlier, the current density for O_2 reduction passed through a maximum with increasing cathodic potentials. This feature has also been observed in alkaline media on the edge orientation of highly oriented graphite and also OPG by Morcos and Yeager[28] and on glassy carbon.[33,34] A possible explanation is the modification of the surface properties, e.g. the reduction of active functional groups, in this potential region. Another possibility is that a step which is to a first approximation potential-independent becomes rate determining. In addition, Morcos and Yeager[28] have demonstrated that the presence of H_2O_2 in the electrolyte modifies the catalytic properties of the graphite surface, and thus it is also possible that peroxide generated at more positive potentials is playing an important role.

At potentials more negative than that corresponding to the minimum shown in Fig. 6, the reduction current again increases, probably because of a change in the pathway by which the graphite surface catalyzes the reduction of oxygen to peroxide. Although some researchers[35-38] have attributed this second reduction wave to further reduction of peroxide, kinetic studies of the O_2 reduction on glassy carbon in alkaline media[33,34] have also demonstrated that only peroxide is generated over the entire potential range examined. It is possible that the differences in the experimental results reported by various researchers may be associated with differences in the catalytic properties of the carbon and graphite surfaces used, variations in the surface preparation, and in a questionable way due to traces of platinum deposited on

the carbon or graphite disk particularly if platinum rather than gold is used as ring and/or counter electrodes.

Oxygen Reduction on FeTPyPz Pre-adsorbed on OPG Surface

Rotating ring-disk O_2 polarization curves in 0.1 M NaOH in the absence and presence of FeTPyPz adsorbed on the OPG surface are shown in Fig. 10. The increase in the rate of O_2 reduction resulting from the presence of the macrocycle is quite considerable, even though OPG by itself is effective for the reduction of O_2 to H_2O_2 in alkaline solutions as previously demonstrated. The potential for the onset of O_2 reduction (~-0.05 V vs. SCE) correlates very well with the voltammetric peak 3 shown in Fig. 3, and this suggests Fe(II)TPyPz as the active form for the catalysis of the reaction.

The polarization curve for the reduction of O_2 by FeTPyPz exhibits an interesting dependence on the applied potential (see Fig. 10). The amount of peroxide detected at the ring for low overpotentials is very small. As the potential is made more negative, the current at the disk decreases and that at the ring increases. At even more negative potentials, the disk current increases again and is followed by a simultaneous decrease in the current associated with the oxidation of peroxide at the ring.

The rotating ring-disk polarization curves for oxygen reduction on FeTPyPz as a function of the rotation rate are shown in Fig. 11. For potentials more positive than that corresponding to the maximum (~-0.5 V vs. SCE), a plot of i^{-1} vs. $f^{-1/2}$ at fixed potentials is shown in Fig. 12. The linearity and parallelism in this plot are as is expected for first order in O_2 according to Eq. 11. The B value obtained from this plot is $(2.92 \pm 0.08)\times10^{-2}$ mA $(rpm)^{-1/2}$, which is in good agreement with the theoretical value 2.85×10^{-2} mA $(rpm)^{-1/2}$, calculated from Eq. 12 for n = 4 and using the same data for the solubility and diffusion coefficient as those previously used for the reduction of O_2 on OPG

in 0.1 M NaOH.

For polarization more negative than -0.5 V vs. SCE, the disk current decreases and reaches a minimum at about .8 V vs. SCE, as shown in Fig. 11. Plots of i^{-1} vs. $f^{-1/2}$ for polarizations in this potential range are shown in Fig. 13. The slopes of the lines (1/B) increase as the potential is made more negative; i.e., the diffusional parameter increases indicating that the number of electrons per O_2 molecules diffusing to the electrode decreases. Thus, the reduction of oxygen also proceeds through generation of peroxide as a reaction product in this potential range, which was also detected at the ring (see Fig. 11).

Figure 14 shows a plot of $(i_d/i_r)N$ vs. $f^{-1/2}$ in the potential region -0.65 V to -0.85 V vs. SCE, where peroxide is detected. The substantial deviation from linear behavior at low values of $f^{-1/2}$ may be caused by eccentricity of the electrode shaft and wobble, the effects of which become more pronounced at higher rotation rates. Independent of whether such deviations are real or an experimental artifact, the data show that the intercepts are potential dependent and greater than unity. Although Damjanovic, Genshaw, and Bockris[39] have considered that intercepts greater than unity are evidence of a parallel mechanism for O_2 reduction, Zurilla, Sen and Yeager[40] have shown that even with only a series mechanism operative and a potential-dependent adsorption-desorption step for H_2O_2, potential-dependent intercepts greater than unity may be obtained. Thus, Fig. 14 does not provide a sufficient criterion to distinguish between the series and the parallel mechanisms. It is interesting to note that the decrease in the disk current, as well as the increase in the ring current, occur at potentials where a second redox process related to the iron center takes place (peak 2 in Fig. 3). This suggests that the further reduced form of the catalyst is ineffective for the 4-electron reduction process. Qualitatively similar behavior was reported by Zagal et al.[7] for FeTsPc

in alkaline media. In addition, the observation of peroxide generation in this potential region also can be attributed to the reduction of oxygen on the bare graphite surface exposed to the solution (see Fig. 10 for comparison) but with FeTPyPz at least in part still supporting the overall 4-electron reduction.

At potentials more negative than -0.8 V vs. SCE in Fig. 11, the disk current starts to increase again and is followed by a decrease in the ring current. Such feature may be related to the reduction of the macrocycle ring (peak 1 in Fig. 3), which occurs in approximately the same potential range. This will be discussed later in more detail.

If a first charge transfer step is the rate determining step (rds) with a uniform Nernst diffusion layer and combined diffusion kinetic control, the current with negligible back reaction is related to the potential E by the relation[18]

$$i = i_o\left(\frac{i_D - i}{i_D}\right)\exp\left[\frac{-\alpha F(E - E_r)}{RT}\right] \qquad (16)$$

where i_o the exchange current density, i_D is the cathodic diffusion limiting current density, E_r is the reversible potential, α the transfer coefficient, and the other terms have their usual meanings. Eq. 16 can be written as:

$$(E - E_r) = \frac{2.3RT}{\alpha F}\left[\log i_o - \log\left(\frac{i \cdot i_D}{i_D - i}\right)\right] \qquad (17)$$

Thus a linear dependence of the potential E on log $[i_D \cdot (i/i_D - i)]$ may be expected under some conditions with the slope (Tafel) corresponding to $-2.3RT/\alpha F$. Figure 15 shows such a plot for the reduction of O_2 on FeTPyPz in 0.1 M NaOH using Eq. 17 with $i_D = 8.8$ mA cm^{-2} for 0.1 M NaOH at 3600 rpm for the 4-electron process, which was calculated from the B value obtained from the slopes of the i^{-1} vs. $f^{-1/2}$ plots shown in Fig. 12. A linear Tafel region with

slope of ~110 mV/decade was obtained over almost two decades of current. This value compares favorably with the expected -120 mV/decade for $\alpha = 0.5$ in Eq. 17, and it implies rate control by an initial one-electron transfer step.

The polarization curves have shown that the onset potential for O_2 reduction takes place in the same region where the redox process given by Eq. 6 occurs. For simplicity, Eq. 6 will be rewritten as:

$$Fe(III)\text{-}OH + e^- = Fe(II) + OH^- \qquad \text{fast} \tag{6a}$$

Assuming an ideal Nernstian behavior for reaction (i) and expressing the surface concentrations of FeTPyPz species in terms of coverage, θ ($0 < \theta < 1$), i.e.,

$$[Fe(II)] = \theta \cdot \Gamma \tag{18}$$

and

$$[Fe(III)\text{-}OH] = (1 - \theta) \cdot \Gamma \tag{19}$$

where Γ is the total surface concentration of FeTPyPz species, the following relation can be obtained:

$$E = E^o - \frac{RT}{F} \ln \frac{\theta\ (OH^-)}{(1 - \theta)} \tag{20}$$

where E^o is the standard electrode potential and (OH^-) represents the solution phase concentration of OH^-. Eq. 20 can be converted to:

$$\theta = \frac{(OH^-)^{-1} \exp[-F/RT\ (E - E^o)]}{\{\ 1 + (OH^-)^{-1} \exp[-F/RT\ (E - E^o)]\}} \tag{21}$$

Eq. 21 gives the surface coverage with active sites, Fe(II)TPyPz, as a function of the potential. Once Fe(II)TPyPz species are generated, the reduction of oxygen starts to take place and the following pathway can be postulated:

$$Fe(II) + O_2 \underset{k'_2}{\overset{k_2}{\rightleftharpoons}} Fe(III)\text{-}O_2^- \qquad \text{fast} \qquad (6b)$$

$$Fe(III)\text{-}O_2 + e^- \xrightarrow[\text{rds}]{k_3} \text{products} \qquad \text{slow} \qquad (6c)$$

Reaction (iii) would then be followed by further fast steps yielding OH^- as the product of the O_2 reduction with a total of 4 e^- per O_2 consumed. For this reaction scheme, the rate of the overall reaction can be expressed in terms of current (i) and given by:

$$i = 4F \cdot k_3 [Fe(III)\text{-}O_2^-] \exp\left[\frac{-\alpha F(E - E^o)}{RT}\right] \qquad (22)$$

Assuming steady state for step (6b), the concentration of $[Fe(III)\text{-}O_2^-]$ adsorbed species is given by

$$[Fe(III)\text{-}O_2^-] = \frac{k_2[O_2]\theta\Gamma - i}{k'_2} \qquad (23)$$

By replacing Eq. 23 in Eq. 22, the following expression for the current can be derived:

$$i = \frac{4F\left(\frac{k_2}{k'_2}\right)k_3[O_2]\theta\Gamma \exp\left[-\frac{\alpha F}{RT}(E - E^o)\right]}{1 + \left(\frac{k_3}{k'_2}\exp\left[\frac{\alpha F}{RT}(E - E^o)\right]\right)} \qquad (24)$$

Equation 24 shows that when $\theta \rightarrow 1$ and the potential dependent term (k_3/k_2') $\exp[\alpha F(E - E^o)\ RT] >> 1$, then the current i becomes a limiting current and is given by:

$$(i_2)_L = 4F \cdot k_2 \cdot [O_2] \cdot \Gamma \qquad (25)$$

or

$$(i_2)_L = 4F \cdot k_2 \cdot \left(\frac{i_D - i}{i_D}\right) \cdot \Gamma \cdot (O_2)_b \qquad (26)$$

where $[O_2]$ is the surface concentration of O_2 and $(O_2)_b$ is the bulk concentration of O_2 in solution.

By replacing Eq. 21 in Eq. 24, as well as including $(i_2)_L$ in the expression, the current becomes:

$$i = (i_2)_L \frac{\left\{ \frac{k_3}{k'_2} (OH^-)^{-1} \exp\left[-(1 + \alpha)\right]Z \right\}}{\left\{ 1 + (OH^-)^{-1} \exp(-Z) \right\} \left[1 + \frac{k_3}{k'_2} \exp(-\alpha Z)\right]} \qquad (27)$$

where $Z = [(F/RT)(E - E^o)]$. This equation predicts that the reaction is first order in O_2 and a limiting current that is directly proportional to the FeTPyPz surface concentration and to O_2 concentration.

According to this proposed mechanism, the steps (6b) and (6c) are fast and slow, respectively. Under such conditions, the term $(OH^-)^{-1}\exp(-Z)$ in the denominator of Eq. 27 predominates, and the rate of the reaction is simply given by:

$$i = (i_2)_L \left(\frac{k_3}{k'_2} \right) \exp\left[- \frac{\alpha F}{RT} (E - E^o)\right] \qquad (28)$$

By replacing Eq. 26 in Eq. 28, the rate of the reaction becomes

$$\left(\frac{i \cdot i_D}{i_D - i} \right) = K \cdot (O_2)_b \cdot \Gamma \cdot \exp\left[- \frac{\alpha F}{RT}(E - E^o)\right] \qquad (29)$$

where $K = [(k_2 \cdot k_3)/ k'_2]$. Thus, a linear Tafel region can be expected with a slope of

$$\left[\frac{d E}{d \log\left(\frac{i \cdot i_D}{i_D - i}\right)} \right] = - \frac{2.3RT}{\alpha F} \qquad (30)$$

or -120 mV/decade at 25°C with $\alpha = 0.5$. Therefore, at polarizations E < -0.5 V vs. SCE, the proposed mechanism predicts the Tafel slope observed experimentally, as well as, a limiting current directly proportional to O_2 concentration and dictated by Fe(II)TPyPz surface concentration. This mechanism is essentially the same as proposed for FeTsPc in alkaline solutions by Zagal, Bindra and Yeager.[7]

THEORETICAL CONSIDERATIONS

From a quantum mechanical viewpoint the voltammetry peaks can be related in a first approximation to the relative positions of the electrode Fermi level with respect to the molecular orbitals of the adsorbate. Specifically, a reduction (or an oxidation) of the adsorbed species can be expected to take place when the electrode Fermi level is shifted upwards (or downwards) past the energy of an empty (or filled) orbital of the adsorbate.

Hence, in the case of FeTPyPz (or FeTsPc), the first two empty orbitals of the ferric species (see Fig. 16) would be mostly iron in character providing support for the assigment of the voltammetry peaks 2 and 3 (see Fig. 3) to redox processes involving the metal center. It should be stressed, however, that the mostly iron d_{z^2} orbital in Fe(I)TPyPz would lie much higher in energy and thus above the $e_g(\pi^*)$ orbitals indicated in Fig. 16. This is due to the less electronegativity of the metal center when in the highly reduced state, an effect that cannot be accounted for by the semi-empirical method used in the molecular orbital calculations.[11]

The proposal that Fe(II)TPyPz, generated at potentials corresponding to the voltammetric peak 3, is the active species that catalyzes the reduction of oxygen is supported by the fact that several iron macrocycles in which the metal center is in the formal oxidation state II have been found to react with O_2 to form μ-oxo species in which the iron centers of two macrocycles are

linked by a single oxygen atom. The most throughly characterized compounds of this type are those derived from iron (II) porphyrins.[41] The formation of similar species in the case of iron phthalocyanines has been infered from a number of measurements including IR spectroscopy[42] and Mossbauer spectroscopy.[43,44] More detailed information on their structure, however, has been hampered by the lack of X-ray crystallographic data. Nevertheless, the fact that ferrous porphyrins, phthalocyanines, and most likely porphyrazines and in fact most ferrous salts in aqueous solutions are indeed capable of reacting with dioxygen leading in some cases to the cleavage of the O=O bond, provides evidence that similar processes may occur at electrochemical interfaces. In the latter case, the electrode can reduce the reaction product and regenerate the catalyst.

Reed[45] reacted Fe(I)TPP$^-$ (TPP = tetraphenyl porphyrin) with O_2 in THF and obtained a solid at room temperature. On the basis of UV-visible, EPR, and Mossbauer spectroscopic information this compound was identified as $(FeTPPO_2)Na$. It is conceivable that the interaction between O_2 and Fe(I)TPyPz may also be favorable and thus facilitate the reduction of O_2. The electrochemical results, however, indicate that the bonding between HO_2 and Fe(I)TPyPz may not be strong leading to the desorption of the peroxide before it can be further reduced, as judged by the detection of peroxide on the ring electrode at more negative potentials.

On the basis of the molecular orbital diagram[45] in Fig. 16, in addition to the voltammetric features denoted as 2 and 3 in Fig. 3, peak 1 appears to involve the strong ring character e_g (π^*) orbitals of FeTPyPz, which have a large p_z orbital contribution from the ring nitrogen atoms. The spatial distribution of the metal d_{xz} orbital and the macrocycle e_g(π^*) orbital

are such that their interaction with O_2 are symmetry allowed (see Fig. 17a and b).

Preliminary molecular orbital calculations[46] have shown that the perpendicular interaction shown in Fig. 17b is more favorable as compared to the side-on geometry depicted in Fig. 17a. Furthermore, the reduction of molecular O_2 would require bond cleavage and formation of intermediates after protonation. Such processes via type a geometry (see Fig. 17a) are more unlikely to occur since it will result in an intermediate with an OH group attached to the inner nitrogen atom. Case b, however, after the dissociation of the O=O bond can produce an intermediate, which could be further stabilized through protonation. Hence, if the electron population of the $e_g(\pi^*)$ orbital is increased by shifting, for instance, the electrode potential beyond peak 1, the back-bonding to the O_2 may lead to the cleavage of the O=O bond. This suggestion of ligand-assisted O_2 reduction appears to support the explanation suggested earlier for the increase in the disk current at potentials more negative than ~-1.1 V vs. SCE and the corresponding decrease in the amount of peroxide detected at the ring.

ACKNOWLEDGEMENTS

The authors express thanks to Professor A. Anderson of Case Western Reserve University for assisting one of the authors (C. Fierro) with the ASED molecular orbital calculations upon which the theoretical discussion section of this paper is based. The authors also acknowledge helpful discussions with Drs. S. Gupta and D. Tryk of Case Western Reserve University and Professor A.B.P. Lever of York University, Toronto. This research has been supported by the U.S. Office of Naval Research and the Department of Energy through a subcontract with the University of California at Berkeley and the Gas Research Institute.

REFERENCES

1. E. Yeager, J. Mol. Catal., 38, (1986) 5.

2. H.-Y. Liu, I. Abdalmuhdi, C.K. Chang, F.C. Anson, J. Phys. Chem., 89 (1985) 665.

3. O. Ikeda, K. Okabayashi, N. Yoshida, and H. Tamura, J. Electroanal. Chem., 191, (1985) 157.

4. R.R. Durand, Jr., C.S. Bencosme, J.P. Collman, and F.C. Anson, J. Am. Chem. Soc., 105, (1983) 2710.

5. H.-Y. Liu, M.J. Weaver, C.-B. Wang, and C.K. Chang, J. Electroanal. Chem., 145, (1983) 439.

6. P.A. Forshey, T. Kuwana, N. Kobayashi, and T. Osa, In Adv. Chem. Ser. No. 201, K.M. Kadish, Ed., American Chemical Society, Washington,(1982) 601.

7. J. Zagal, P. Bindra and E.B. Yeager, J. Electrochem. Soc., 127, (1980) 1506.

8. F. van der Brink, E. Barendrecht, and W. Visscher, J. Royal Neth. Chem., 99, (1980) 253.

9. M.R. Tarasevich and K.A. Radyushkina, Russ. Chem. Rev., 49, (1980) 718.

10. J. Zagal, R.K. Sen, and E. Yeager, J. Electroanal. Chem., 83, (1977) 207.

11. C. Fierro, A. Anderson, and D. Scherson, J. Phys. Chem. (in press).

12. a) S. Zecevic, B. Simic-Glavaski, E. Yeager, A.B.P. Lever, and P.C. Minor, J. Electroanal. Chem., 196, (1985) 339. b) B. Simic-Glavaski, S. Zecevic and E. Yeager, J. Am. Chem. Soc., 107 (1985) 5625.

13. T.D. Smith, J. Livorness, H. Taylor, J.R. Pilbrow, and G. R. Sinclair, J. Chem. Soc. Dalton Trans., (1983) 1391.

14. J.H. Weber and D.H. Busch, Inorg. Chem., 4, (1965) 469.

15. W.J. Albery and S. Bruckenstein, Trans. Faraday Soc., 62, (1966) 1920.

16. J. Zagal, Ph.D. Thesis, Department of Chemistry, Case Western Reserve University, Cleveland, Ohio, 1977.

17. The apparatus and technique is a modified version by Dr. B. Cahan of a system previously report by R. Gilmont and S.J. Silvis, Am. Lab., 6, (1974) 46.

18. A.J. Bard and L.R. Faulkner, in "Electrochemical Methods-Fundamental and Applications", John Wiley & Sons, New York, 1980, p.7, 110, 521.

19. J.-P. Randin and E. Yeager, J. Electroanal. Chem., 36, (1972) 257.

20. H.H. Bauer, M.S. Spritzer, and P.J. Elving, J. Electroanal. Chem., 17, (1968) 299.

21. R.F. Pasternack, H. Lee, P. Malek and C. Spencer, J. Inorg. Nucl. Chem., 39, (1977) 1865.

22. P.A. Forshey and T. Kuwana, Inorg. Chem., 20, (1980) 693.

23. W.A. Nevin, W. Liu, M. Melnic and A.B.P. Lever, J. Electroanal. Chem., 213, (1986) 217.

24. A.B.P. Lever and J.P. Whilshire, Can. J. Chem., 54, (1976) 2514.

25. A.B.P. Lever and J.P. Wilshire, Inorg. Chem.,. 17, (1978) 1145.

26. E.B. Fleischer, J.M. Palmer, T.S. Srivastava, and A. Chatterjee, J. Am. Chem. Soc., 93, (1971) 3162.

27. J. Koutecky and V.C. Levich, Zh. Fiz. Khim., 32, (1958) 1565.

28. I. Morcos and E. Yeager, Electrochim. Acta, 15, (1970) 953.

29. C.-W. Lee, H.B. Gray, F.C. Anson, and B.G. Malmstrom, J. Electroanal. Chem., 172, (1984) 289.

30. J. Newman, J. Phys. Chem., 70, (1966) 1327.

31. K.E. Gubbins and R.D. Walker Jr., J. Electrochem. Soc., 112, (1965) 469.

32. H.S Wroblowa, Y.-C. Pan, and G. Razumney, J. Electroanal. Chem., 69, (1976) 195.

33. M.S. Hossain, Ph.D. Thesis, Department of Chemistry, Case Western Reserve University, Cleveland, Ohio, 1986.

34. R.J. Taylor and A.A. Humffray, J. Electroanal. Chem., 64, (1975) 63.

35. a) M.R. Tarasevich, F.Z. Sabirov, A.P. Mertsalova, and R.K. Burshtein, Elektrokhimiya, 4, (1968) 432; b) F.Z. Sabirov and M.R. Tarasevich, Elektrokhimiya, 5, (1969) 608; c) M.R. Tarasevich and F.Z. Sabirov, Elektrokhimiya, 5, (1969) 643; d) M.R. Tarasevich, F.Z. Sabirov, and R.K. Burshtein, Elektrokhimiya, 7, (1971) 404.

36. M. Brezina and A. Hofmanova, Collect. Czech. Chem. Commun., 38, (1973) 985.

37. N.M. Zagudaeva, V.S. Vilinskaya, and G.V. Shteinberg, Elektro- khimiya, 18, (1982) 541.

38. B. Lovrecek, M. Batinic, and J. Caja, Electrochim. Acta, 28, (1983) 685.

39. A. Damjanovic, M.A. Genshaw, and J.O'M. Bockris, J. Electroanal. Chem., 15, (1967) 173.

40. R.W. Zurilla, R.K. Sen, and E. Yeager, J. Electrochem. Soc., 125, (1978) 1103.

41. J.W. Buchler, in "Porphyrins and Metalloporphyrins", K.M. Smith, Ed., Chapter 5, Elsevier, New York, 1975, p.157.

42. C. Ercolani, M. Gardini, F. Monacelli, G. Pennesi, and G. Rossi, Inorg. Chem., 22, (1983) 2584, and references therein.

43. C. Ercolani, M. Gardini, K.S. Murray, G. Pennesi, and G. Rossi, Inorg. Chem., 25, (1986) 3972, and references therein.

44. A.A. Tanaka, C. Fierro, D. Scherson and E.B. Yeager, J. Phys. Chem., 91 (1987) 3799.

45. C.A. Reed, in Adv. Chem. Ser., No. 201, K.M. Kadish, Ed., Am. Chem. Soc., Washington, (1982) 333.

46. C.A. Fierro, A.A. Tanaka, D. Scherson, and E.B. Yeager, unpublished results.

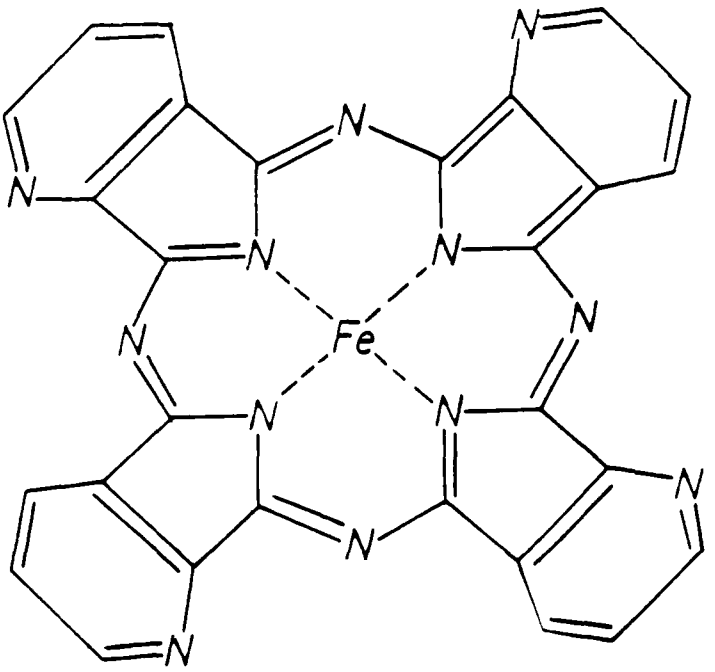

Figure 1. Structure of Iron Tetra-2-3-pyridinoporphyrazine (FeTPyPz).

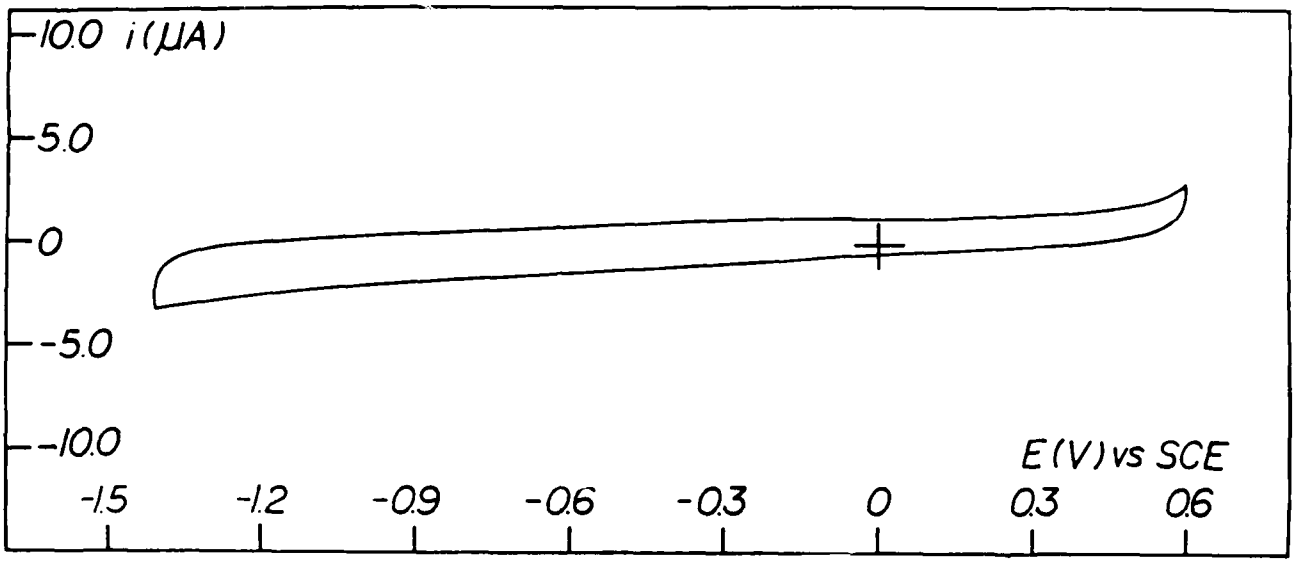

Figure 2. Cyclic voltammogram of an ordinary pyrolytic graphite (OPG) in N_2 saturated 0.1 M NaOH solution at room T. Electrode area = 0.196 cm^2, v = 100 mV s^{-1}.

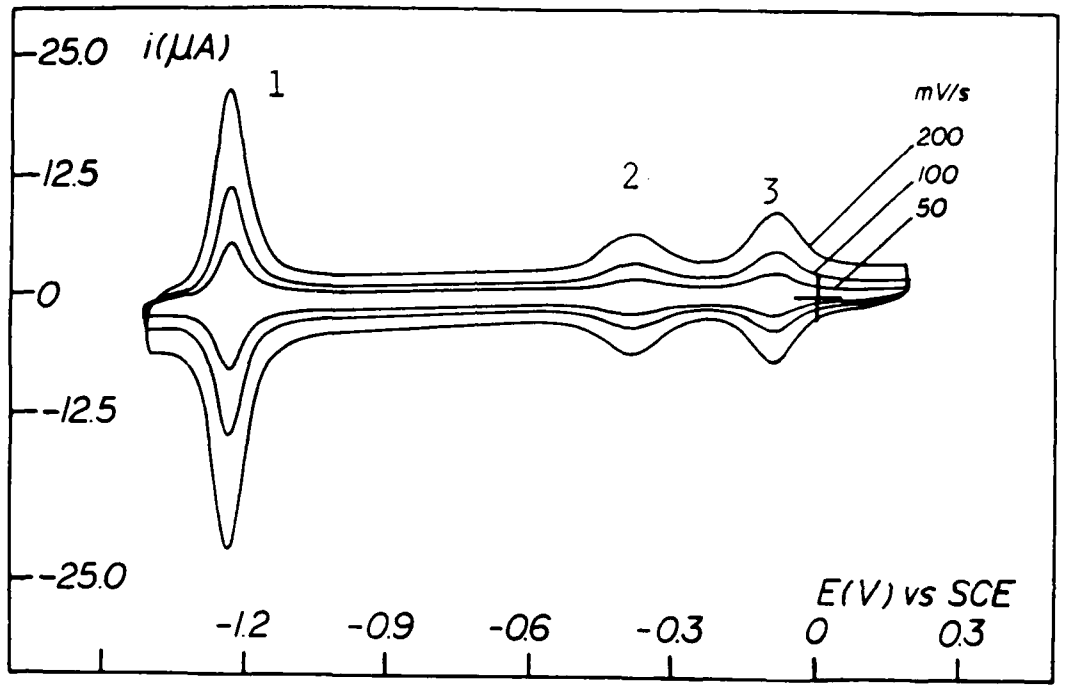

Figure 3. Cyclic voltammograms at different scan rates for FeTPyPz adsorbed on OPG electrode in N_2 saturated 0.1 M NaOH solution at room T.

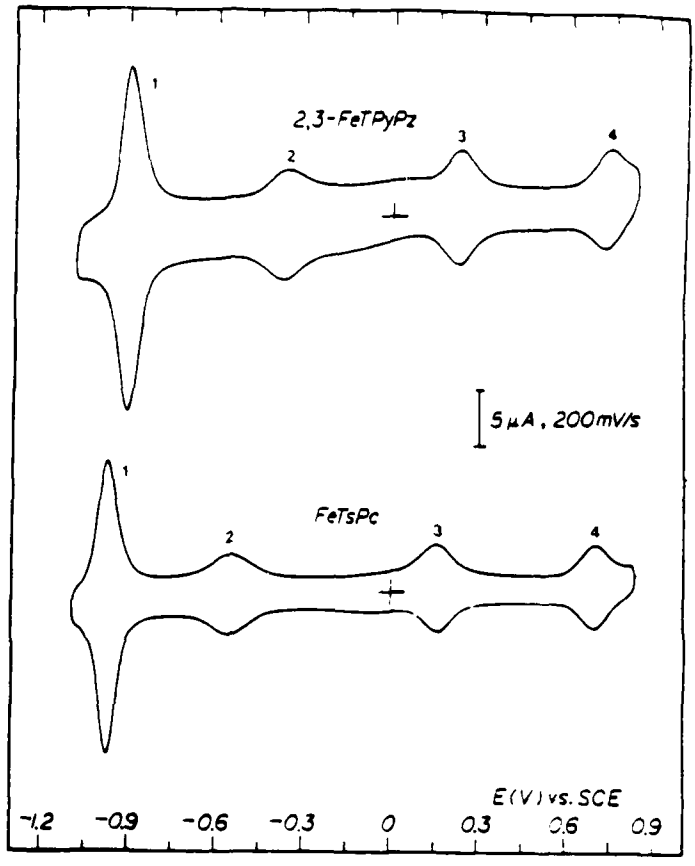

Figure 4. Cyclic voltammograms of adsorbed FeTPyPz (top) and 10^{-5} M FeTsPc (bottom) in borate buffer (pH = 8.4) solution saturated with N_2. OPG substrate area = 0.196 cm^2, room T, v = 200 mV/s.

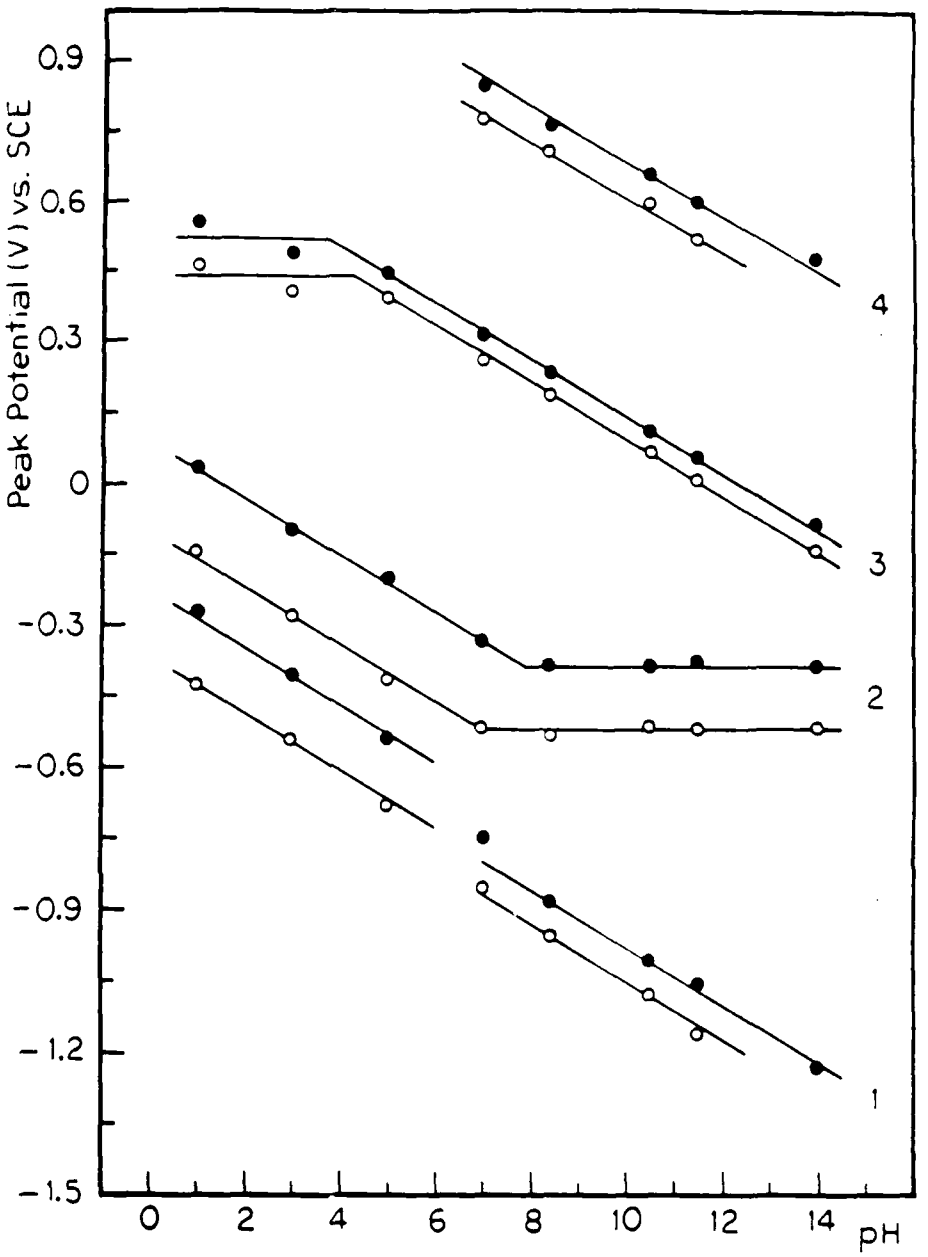

Figure 5. Dependence of the voltammetric peak potentials shown in Fig. 4 with pH for FeTPyPz adsorbed (●) and 10^{-5} M FeTsPc (O) in aqueous solutions saturated with N_2. OPG substrate.

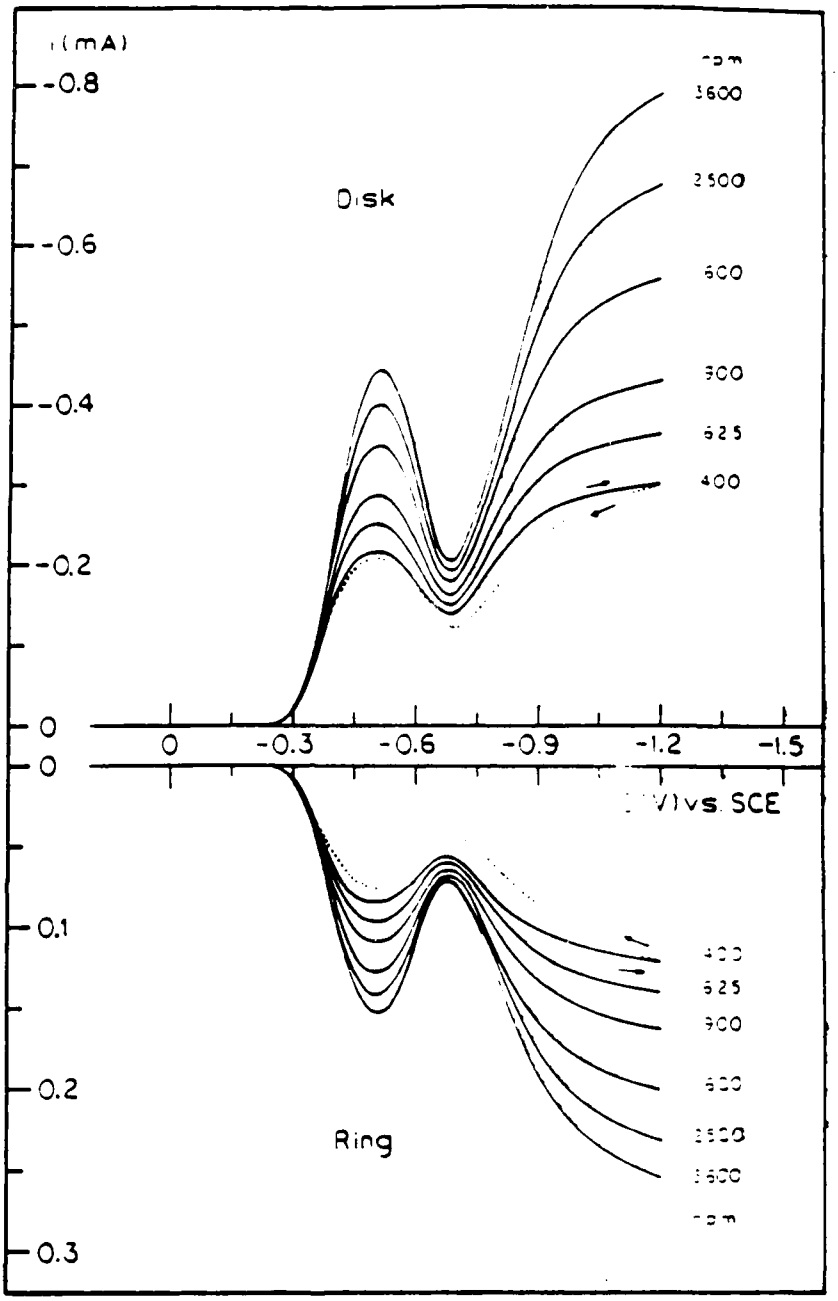

Figure 6. Rotating ring-disk polarization curves for O_2 reduction on OPG in 0.1 M NaOH solution saturated with O_2. OPG electrode area = 0.196 cm^2, room T, v = 10 mV/s. Gold ring (N = 0.38) at +0.1 V vs. SCE.

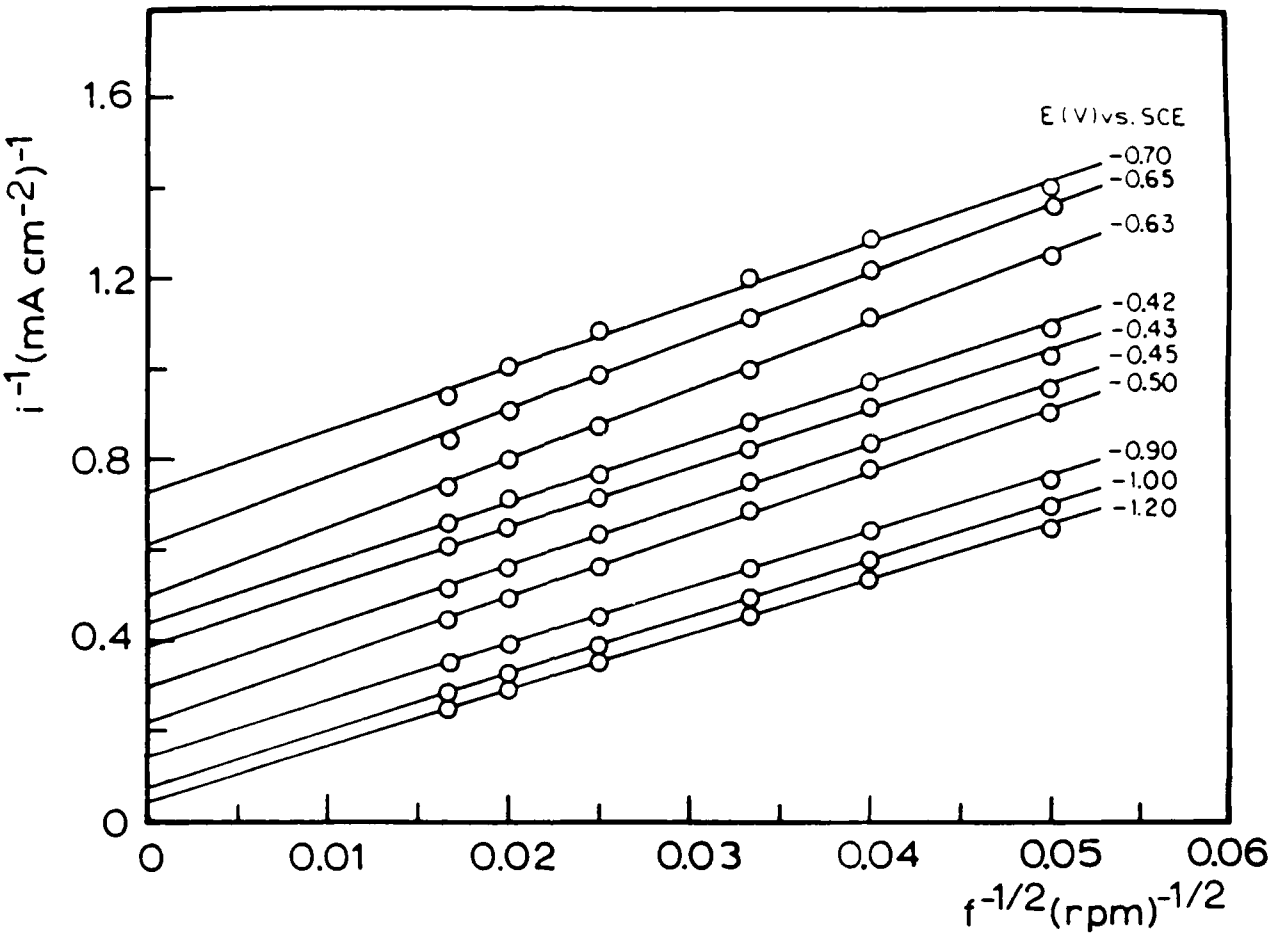

Figure 7. Plot of i^{-1} vs. $f^{-1/2}$ for O_2 reduction on OPG in 0.1 M NaOH solution at different potentials. Data taken from Fig. 6.

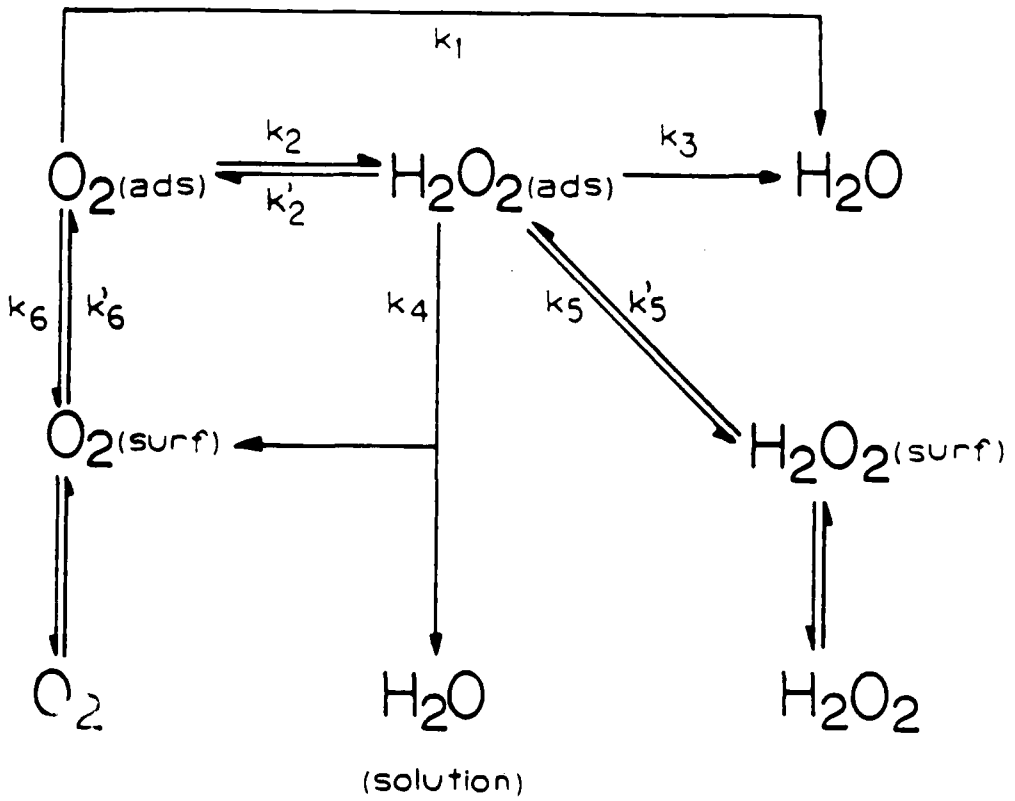

Figure 8. Reaction scheme for O_2 reduction used for the analysis of rotating ring-disk data.

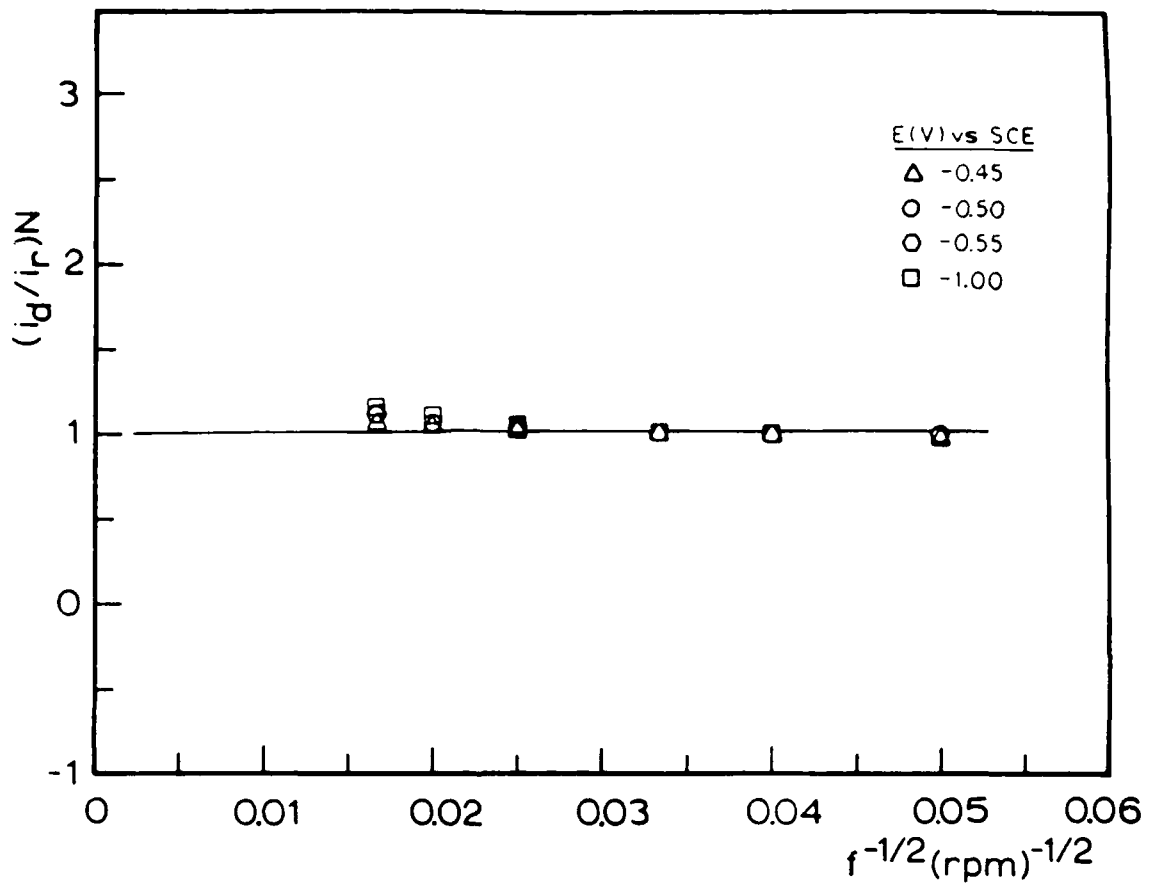

Figure 9. Plot of $(i_d/i_r)\cdot N$ vs. $f^{-1/2}$ for O_2 reduction on OPG in 0.1 M NaOH at various fixed potentials. Data taken from Fig. 6.

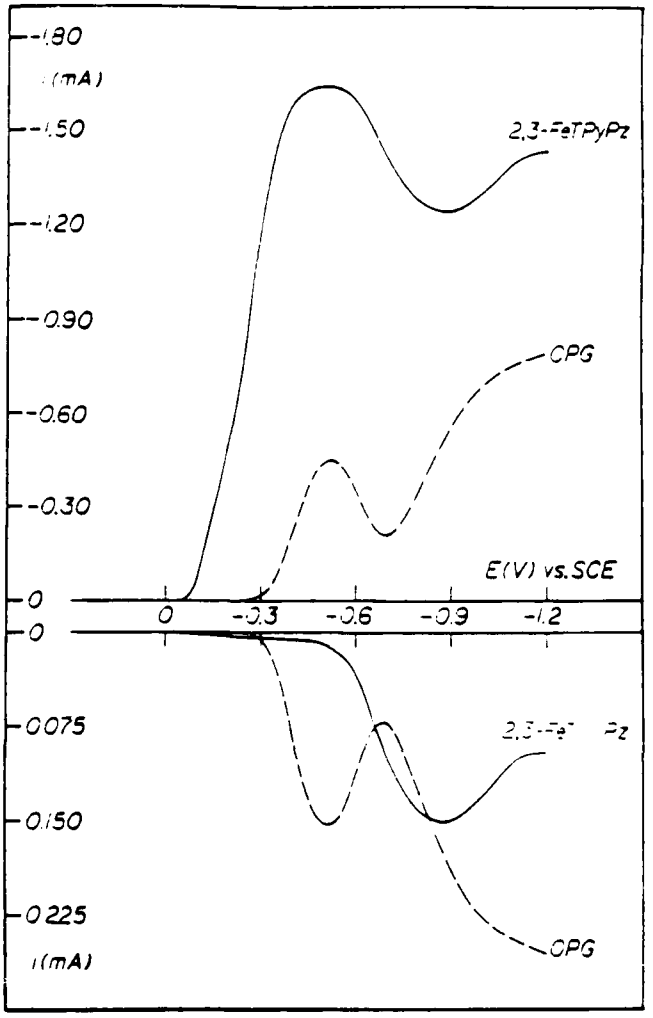

Figure 10. Ring-disk polarization curves for O_2 reduction on OPG (- - -) and on FeTPyPz adsorbed on OPG (——) in 0.1 M NaOH solution saturated with O_2. Electrode area = 0.196 cm^2, room T, v = 10 mV/s, ω = 2500 r.p.m., Au ring (N = 0.38) at +0.1 V vs. SCE.

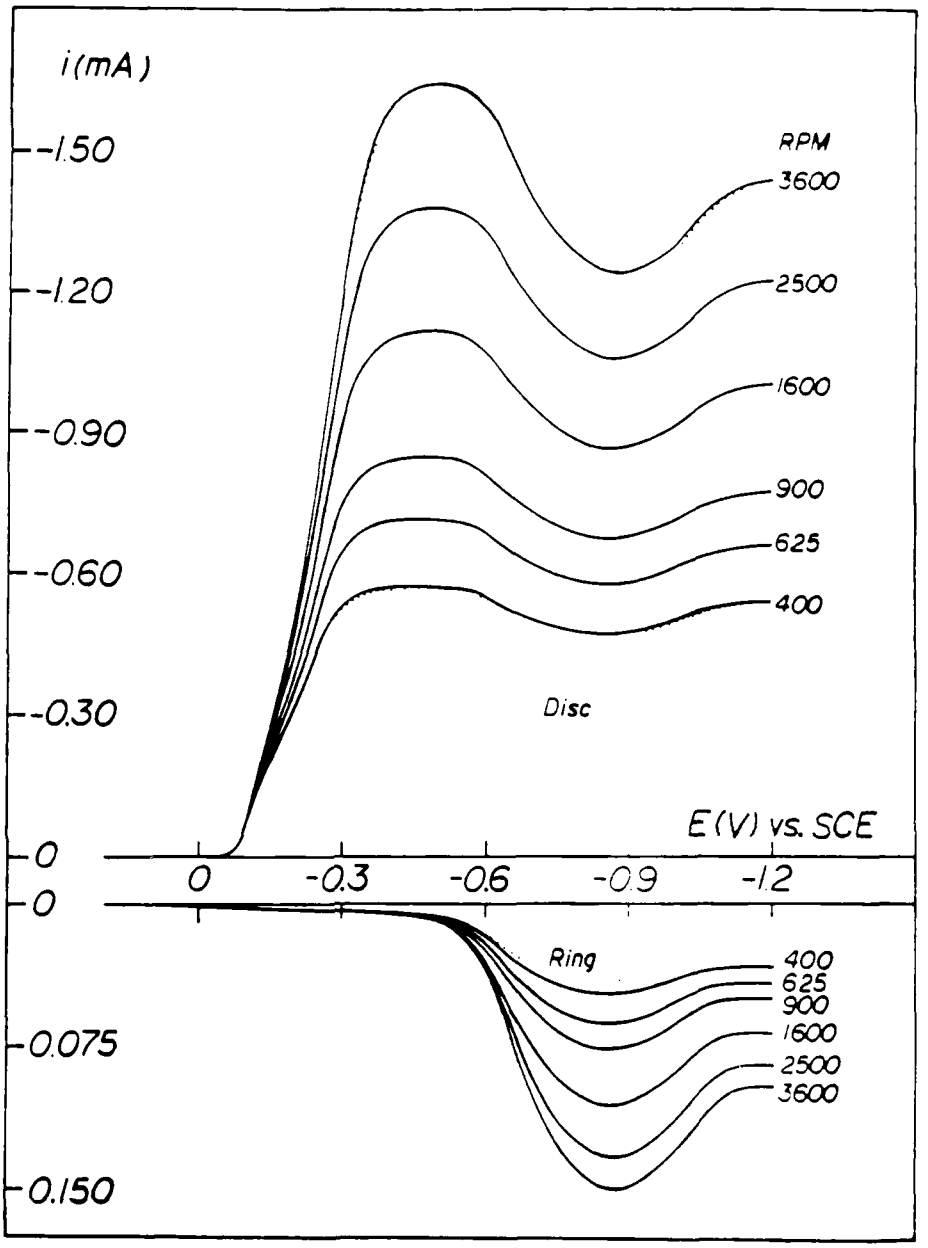

Figure 11. Ring-disk polarization curves at different rotation rates for O_2 reduction on FeTPyPz adsorbed on OPG in 0.1 M NaOH solution saturated with O_2. Electrode area= 0.196 cm^2, room T, v = 10 mV/s, Au ring (N = 0.38) at +0.1 V vs. SCE.

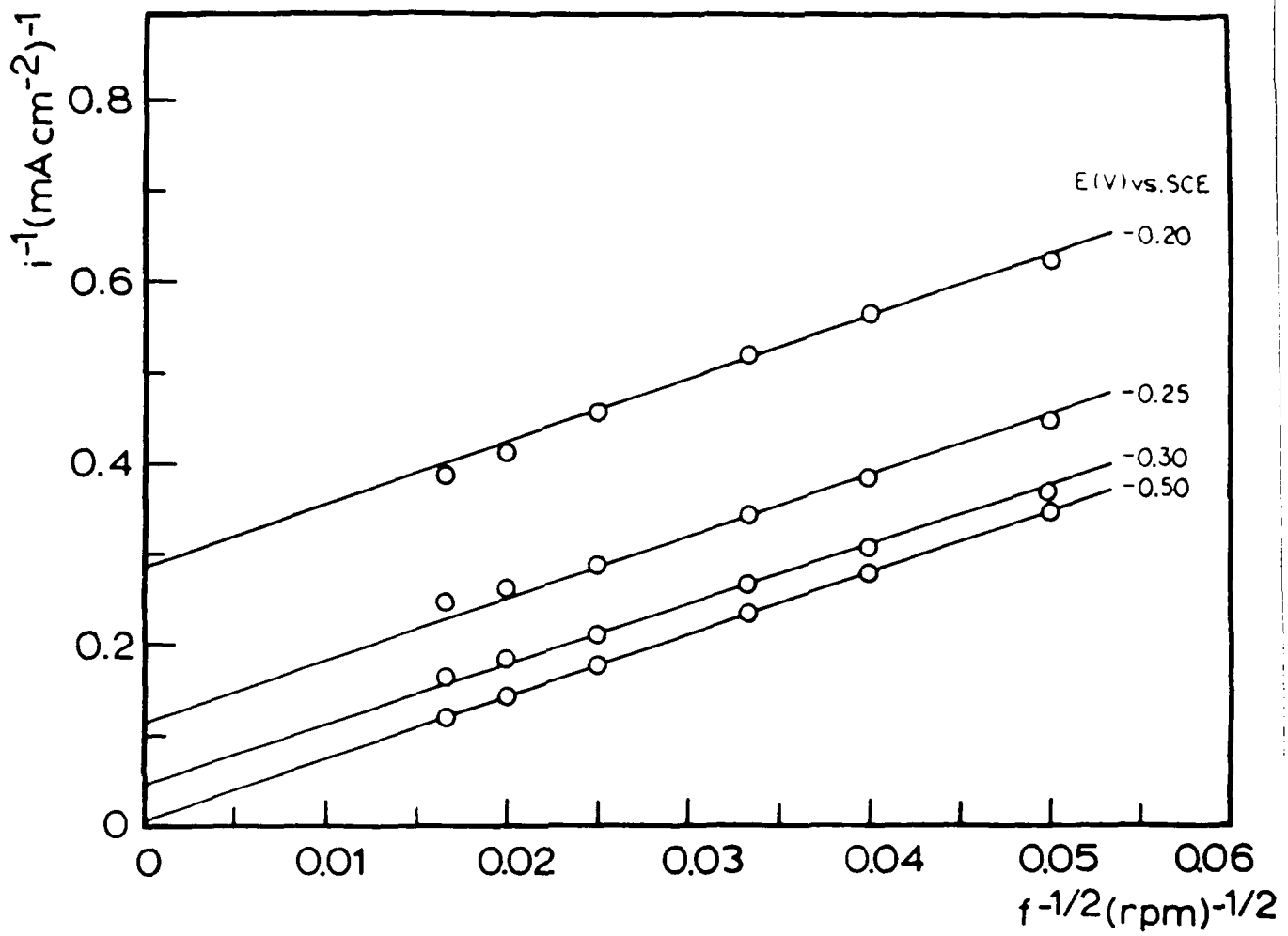

Figure 12. Plot of i^{-1} vs. $f^{-1/2}$ for O_2 reduction on FeTPyPz adsorbed on OPG in 0.1 M NaOH solution saturated with O_2 at potentials more anodic than -0.5 V vs. SCE. Data taken from Fig.11.

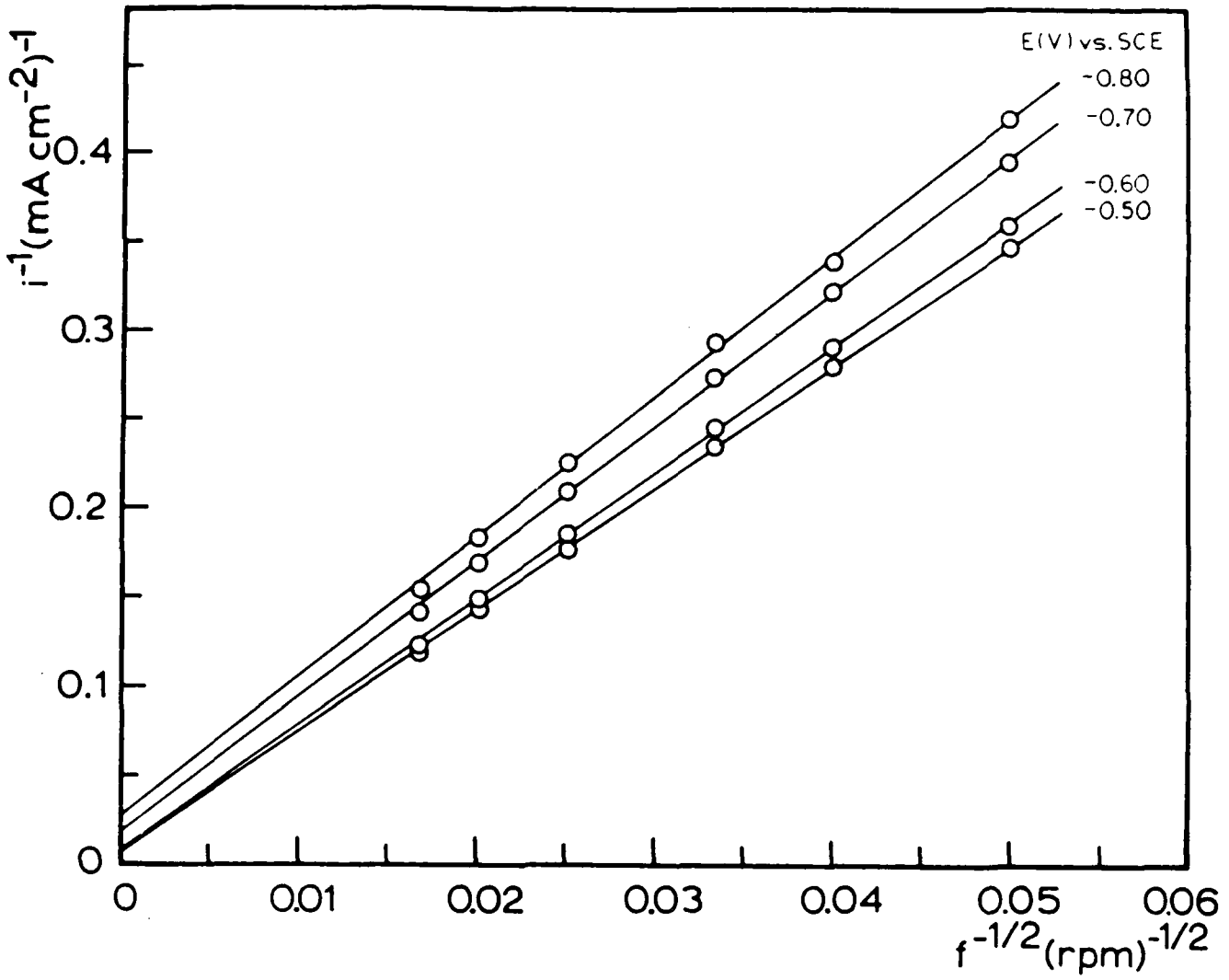

Figure 13. Plot of i^{-1} vs. $f^{-1/2}$ for potentials in the region -0.5 to -0.9 V vs. SCE for O_2 reduction on FeTPyPz adsorbed on OPG in 0.1 M NaOH solution. Data taken from Fig. 11.

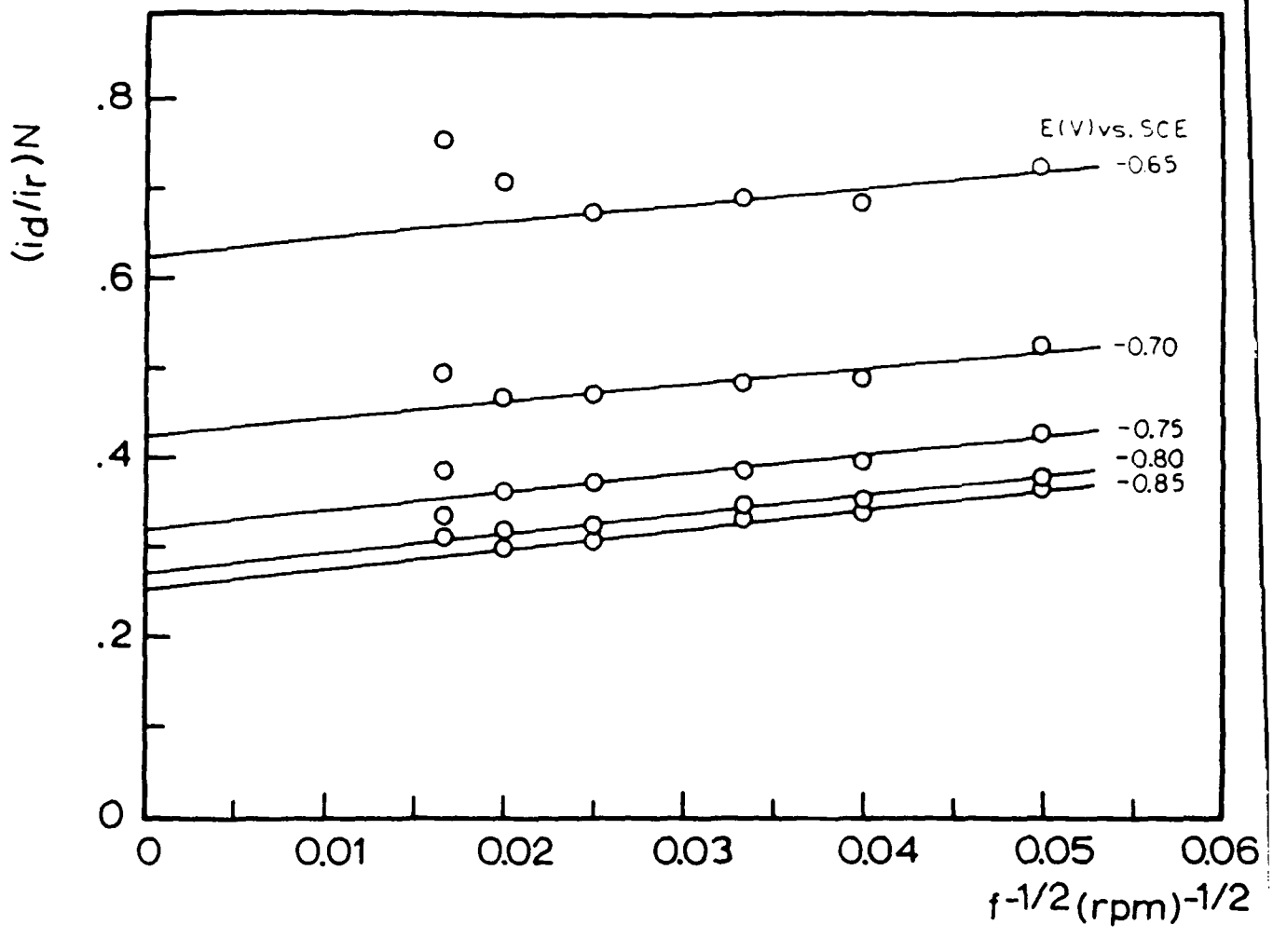

Figure 14. Plot of $(i_d/i_r)N$ vs. $f^{-1/2}$ for potentials in the region -0.5 to -0.9 vs. SCE for O_2 reduction on FeTPyPz adsorbed on OPG in 0.1 M NaOH solution. Data taken from Fig. 11.

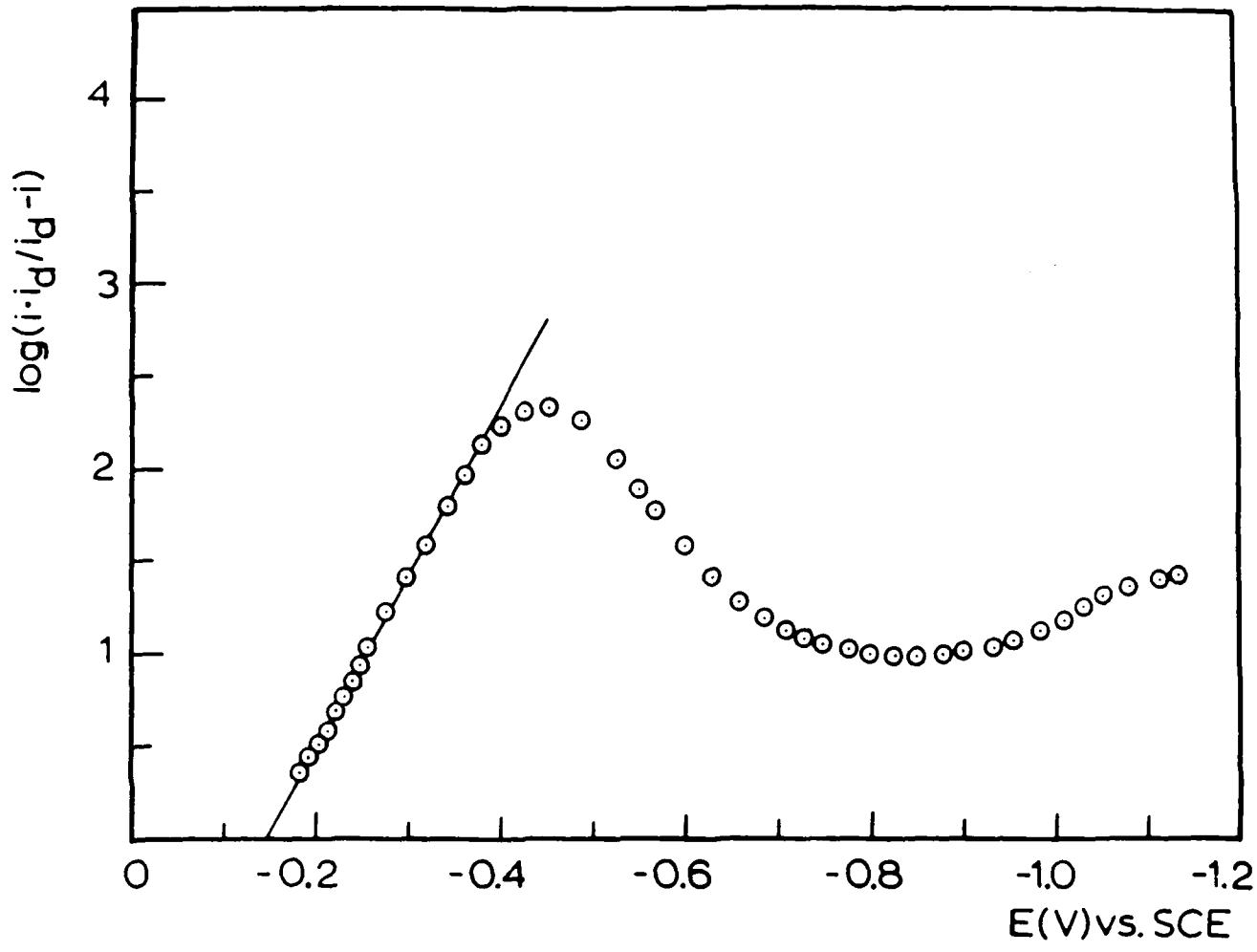

Figure 15. Tafel plot for O_2 reduction on FeTPyPz adsorbed on OPG in 0.1 M NaOH solution saturated with O_2. i_d = 8.8 mA cm^{-2}. f = 3600 rpm. Data taken from Fig. 11.

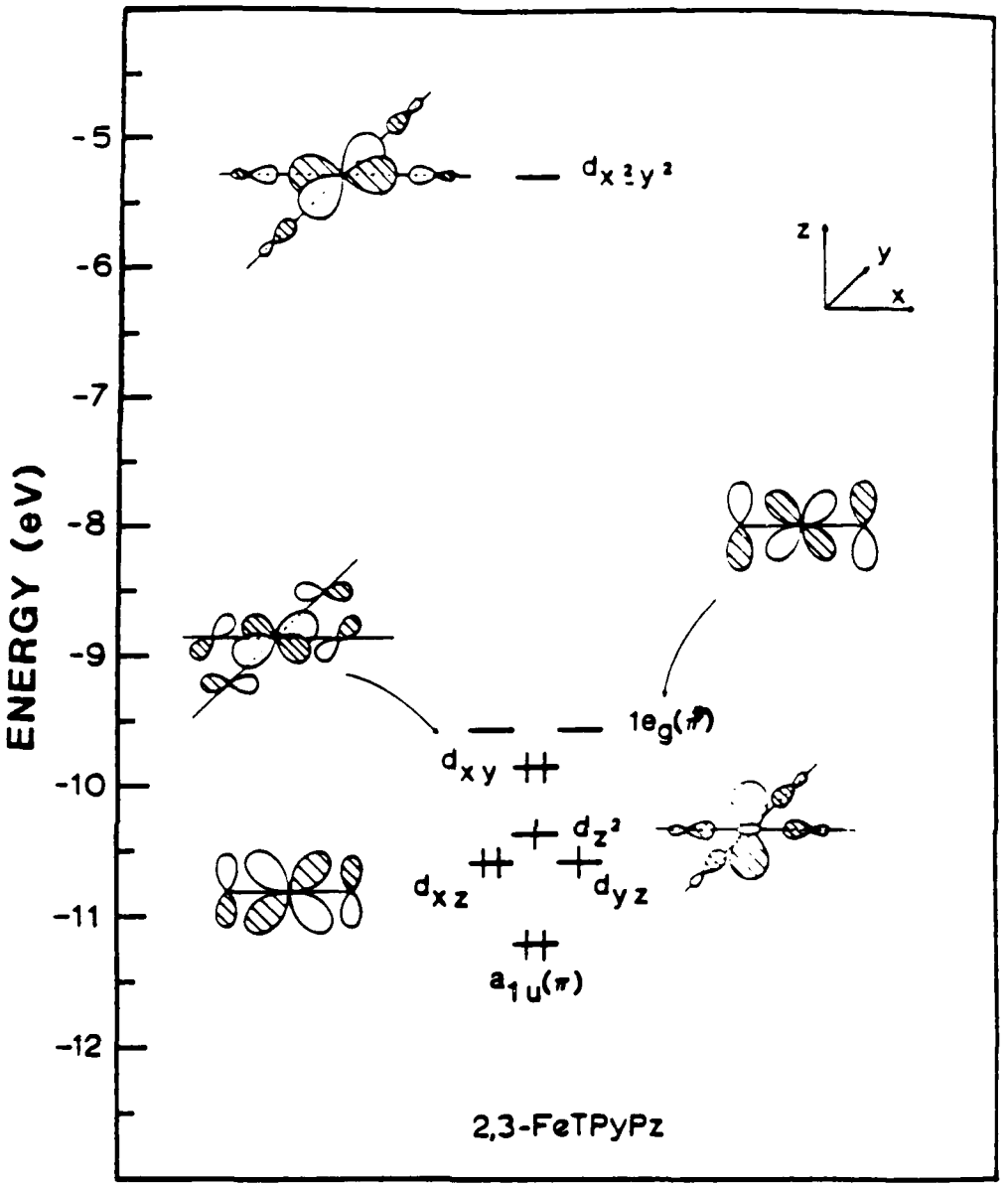

Figure 16. Molecular orbital diagram for FeTPyPz.[46]

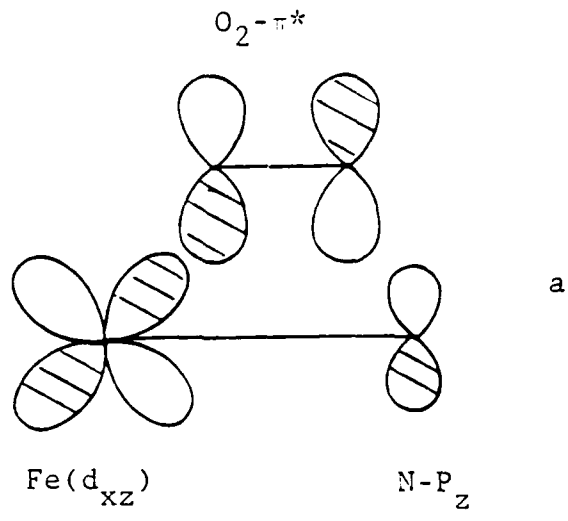

a

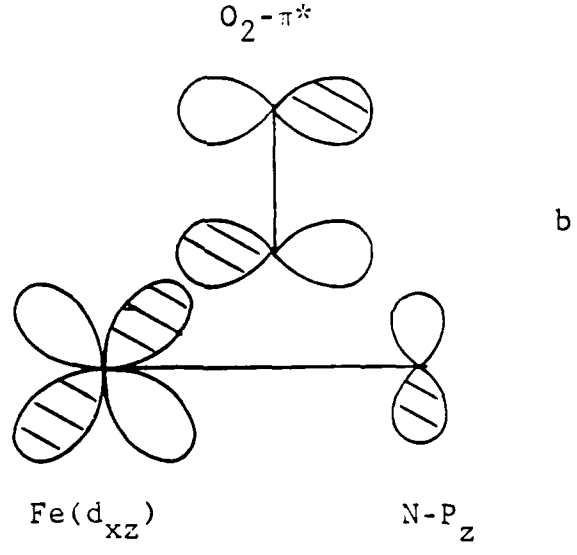

b

Figure 17. Possible bridge-interaction of O_2 with iron and one of the nitrogen in the ring (see text).[46]